Flexible PVDF-TrFe Piezoelectric Energy Harvesters for Structural Health Monitoring Applications in Wind Turbines

by

Berkay Kullukçu

A Dissertation Submitted to the
Graduate School of Sciences and Engineering
in Partial Fulfillment of the Requirements for
the Degree of

Master of Science

in

Mechanical Engineering

KOÇ ÜNİVERSİTESİ

August, 2022

Flexible PVDF-TrFe Piezoelectric Energy Harvesters for Structural Health Monitoring Applications in Wind Turbines

Koç University
Graduate School of Sciences and Engineering
This is to certify that I have examined this copy of a master's thesis by

Berkay Kullukçu

and have found that it is complete and satisfactory in all respects,
and that any and all revisions required by the final
examining committee have been made.

Committee Members:

____
Asst. Prof. Dr. Levent Beker (Advisor)

____
Prof. Dr. Erdem Alaca

____
Assoc. Prof. Dr. Güllü Kızıltaş Şendur

Date: ______________________

To my Family and Friends

ABSTRACT

Flexible PVDF-TrFe Piezoelectric Energy Harvesters for Structural Health Monitoring Applications in Wind Turbines
Berkay Kullukçu
Master of Science in Mechanical Engineering
August, 2022

The field of microelectronics has made tremendous advancements, resulting in the emergence of various electronic devices that have become commonplace in daily life. The continual advancement of energy harvesting technologies has reduced these devices' cost, size, weight, and power needs therefore, the formation of distributed environments, has been made feasible as a consequence of this. The existing energy storage capacity continues to be the major factor in determining the size, mass, and cost of modern electronic equipment. This is because the rate of technical advancement is substantially slower than in the past. Batteries typically lead people to be worried about the influence that their disposal has on the environment as well as the feasibility of replacing them in systems. Because of this difficulty, there was a substantial growth in interest in the solutions of energy harvesting, which are predicted to address the challenges that are brought on by the energy sources utilized in electronic devices. This thesis introduces a flexible piezoelectric energy harvester that could be used for monitoring structural health.

Recent energy costs and efforts to reduce emissions necessitate advancements in renewable energy technology. Due to the inability to use sensors in harsh environments, modern wind turbine instrumentation is expensive and frequently employs indirect measuring techniques. Health monitoring technologies for the establishment of a distributed sensor network can be used to increase productivity and reduce emissions while ensuring safety. The most recent SHM systems have low-power sensors and wireless communication components, both of which can be powered by the outputs of energy harvesters. It is possible to obtain energy from the environment around autonomous sensor systems, which can then be used to power the systems.

In the thesis, a flexible piezoelectric wind energy harvester will be presented. The piezoelectric sensor layer was constructed with polyvinylidene fluoride- trifluoroethylene (PVDF-TrFE). Fabrication, characterization, and modeling of piezoelectric energy harvesters (PEHs) will be discussed. Two different piezoelectric energy harvesting devices were designed and compared. The output voltage and current characteristics were analyzed in a wind test apparatus. The electrical, mechanical, and chemical properties of the PVDF-TrFE material were examined. The harvester's output power and current values were sufficient to power a MEMS pressure sensor with a maximum of 291.34 µA for current and 937.01 mV for voltage under wind pressure, resulting in a power value of 272.99 µW.

ÖZETÇE

Rüzgar Türbini Yapısal Sağlık Kontrol Uygulamaları için Esnek PVDF-TrFe Piezoelektrik Enerji Hasatçısı

Berkay Kullukçu
Makine Mühendisliği, Yüksek Lisans
Ağustos, 2022

Mikroelektronik cihazlar, günlük yaşamda sıklıkla kullanılmaya başlanan çok sayıda yeni elektronik cihazın son yıllarda piyasaya sürülmesiyle sonuçlanan muazzam bir ilerleme kaydetmiştir. Enerji hasadı teknolojilerindeki sürekli gelişmeler cihazların maliyetlerini, boyutlarını, ağırlıklarını ve güç gereksinimlerini azaltarak kablosuz sensör ağları gibi dağınık sistemlerin oluşturulmasına yol açmıştır. Bununla birlikte, mevcut pil teknolojisi yavaş inovasyon hızı nedeniyle mikroelektronik cihazlarin ölçeğini, ağırlığını ve maliyetini belirlemekte en önemli etken olmaya devam etmektedir. Piller, çevresel etkilerinden ve dağınık veya gömülü sistemlerde pil değiştirmenin zorluğundan dolayı çözülmesi gereken bir problem olarak mikroelektronik cihaz tasarımının önünde durmaktadır. Bunun bir sonucu olarak, elektronik cihazlarda sabit kapasiteli enerji kaynaklarının neden olduğu sorunları çözmesi beklenen enerji hasadı teknolojilerine ilgi duyulmaya başlanmıştır. Bahsedilen problemlere çözüm getirmek amacı ile bu tezde, yapısal sağlık kontrolü uygulamaları için bir piezoelektrik enerji hasatçısı (PEH) ve özgün üretim akışı sunulacaktır. Proje hedefi, geliştirilen özgün fabrikasyon akışı ile PEH'i elektrik karakterizasyon testlerinden geçirmek, paketlemesini ve elektronik entegrasyonunu sağlamak ve PEH'in, cihazların içerisinde bulunan pillerin ömürlerini uzatacak fayda sağladığını, testler sonucunda alınacak değerler ile göstermektir.

Günümüzde enerji maliyetlerindeki artış ve daha düşük karbon emisyonuna olan yönelim, yenilenebilir enerji teknolojisinde ilerlemeleri zorunlu kılmaktadır. Zorlu ortamlarda birçok sensörün kullanılamaması nedeniyle, son teknoloji rüzgar türbini enstrümantasyonunun maliyeti yüksektir. Bu enstrümanlar ile birlikte dolaylı ölçüm prosedürleri kullanılmaktadır. Güvenliği sağlarken verimliliği artırmak ve emisyonları en aza indirmek için, dağıtılmış bir sensör ağı ile birlikte yapısal sağlık izleme yöntemlerinden yararlanılabilir. Yeni yapısal sağlık izleme sistemleri, enerji hasatçılarından elde edilen enerji kullanılarak çalıştırılabilen düşük güçlü sensörler ve kablosuz iletişim bileşenleri içermektedir. Bağımsız sensör sistemlerine güç sağlamak için ortamda halihazırda bulunan kaynaklardan enerji elde etmek mümkündür.

Bu tezde esnek bir piezoelektrik enerji hasatçısı sunulmuştur. Piezoelektrik sensör katmanı için, polivinilidin florür-trifloroetilenden (PVDF-TrFE) kullanılmıştır. Tezde piezoelektrik enerji hasatçılarının; fabrikasyon, karakterizasyon ve matematiksel modelleme kısımları açıklanacaktır. İki farklı piezoelektrik enerji hasatçısı tasarlanmış ve farklı parametreler ile karşılaştırılmıştır. Bir rüzgar testi düzeneğinde çıkış voltajı ve akım karakteristikleri incelenmiştir. PVDF-TrFE malzemesinin elektriksel, mekanik ve kimyasal özellikleri incelenmiştir. Hasatçının sağladığı maksimum güç, akım ve gerilim değerleri rüzgar basıncı altında sırasıyla 272.99 μW, 291.34 μA ve 937.01 mV'dir. Bu değerler rüzgar türbini yapısal sağlık kontrol uygulamalarında kullanılacak bir MEMS basınç sensörünü çalıştırmak için yeterlidir.

ACKNOWLEDGMENTS

Koç University's incredible diversity of intellect, culture and research has opened my mind to the possibilities that the future holds for us and the critical role scientists play in molding that future. During my time here, I have had the incredible privilege of meeting many people who are considerably more intelligent and driven than I am, coming from different parts of the world and all walks of life.

I want to express my gratitude to my advisor, Levent Beker, for his advice and assistance over the last two years. Throughout this work, I have learned much from his suggestions and observations. I would like to thank him for showing his students how to face difficulties with passion while preserving a sense of balance in their lives and encouraging them to do the same. I have realized how important his input is to my studies. I have come to appreciate his efficiency, technical depth, and style, and I aspire to be able to duplicate these qualities in the future. As an engineer, his group has been a fantastic place to be.

Thanks to my BMDL lab colleagues for all the laughter. Your friendship, support, and engineering expertise are greatly appreciated. Being part of a team that works on diverse projects has been incredible.

I also like to express my gratitude to the Scientific and Technological Research Council of Türkiye (TUBITAK) for supporting my research under BIDEB 2210-C National MSc/MA Scholarship Program in the Priority Fields in Science and Technology.

Finally, I would like to express my gratitude to my family and friends. Thank you so much for your constant love, support, and encouragement.

TABLE OF CONTENTS

LIST OF TABLES

LIST OF FIGURES

ABBREVIATIONS

WSN	Wireless Sensor Nodes
MEMS	Microelectromechanical Systems
SHM	Structural Health Monitoring
RF	Radio Frequency
PV	Photovoltaic
LED	Light Emitting Diode
DC	Direct Current
LI-ION	Lithium-Ion
TEG	Thermoelectric Generator
GPS	Global Positioning System
RTLS	Real-time locating system
IoT	Internet of Things
BSN	Body Sensor Network
CFPG	Coulomb-Force Parametric Generator
RFID	Radio Frequency Identification
PEH	Piezoelectric Energy Harvester
EEHF	Effective Energy Harvesting Framework
SPEH	Sandwich Piezoelectric Energy Harvester
MSPEH	Multi-Branch Sandwich Piezoelectric Energy Harvester
dB	Decibel
CMOS	Complementary Metal Oxide Semiconductor
FEM	Finite Element Modelling
RPM	Revolution per Minute

Chapter 1

INTRODUCTION

1.1 Introduction

Microelectronics' inclusion and rapid development have profoundly impacted human society in recent decades. The widespread availability of intelligent electronic devices paved a way for a surge of varied applications that may improve one's quality of life in a variety of different ways. Concurrent advancements in microelectromechanical systems (MEMS) technologies have resulted in improved device performance with reductions in size, cost, and the amount of power they use. Together with advancements in the capacity of wireless transmission, the tendency toward devices that are both smaller and inexpensive makes it feasible to establish distributed networks. Such networks have the potential to serve a variety of functions. Observing temperature, light, and the position of individuals in commercial properties to regulate the environment in a manner that is more energy-efficient, detecting dangerous chemical agents in high-density areas, monitoring the formation of fatigue cracks on aircraft, monitoring the speed and pressure in vehicle tires, and a great deal more are all examples of the many applications of this technology. Numerous experts believe that very low-power embedded electronic devices will become ubiquitous, performing tasks ranging from factory automation to entertainment. However, the performance of such new advancements is reliant on the availability of reliable sources of energy in the near future. Batteries and other types of energy sources that have a set capacity present a number of challenges due to their cost, size, and longevity.

Microelectronics has progressed significantly, resulting in an abundance of innovative electronic devices that have become ubiquitous daily. The price, dimensions, weight, and power needs of these devices have all been steadily lowered due to continuous advancements in MEMS technology, which has made it possible to construct distributed systems including WSN [1]. The current battery technology has restrictions on the devices' maximum size, weight, and cost because of the substantially slower pace at which it advances. There is a great deal of uncertainty about both the effect that used batteries have on the nature and the practicability of finding alternatives to using them in systems. Because of this problem, there seems to be a rise in interest in the development of energy harvesting technologies, that are predicted to resolve the issues that are brought about by the usage of energy sources in electronic devices [2]. Sensors, actuators, transmitters, receivers, and processors, all highly integrated intelligent electronic devices, have paved the way for various new life-improving applications. The development of technology known as microelectromechanical systems, or MEMS, has led to improvements in the functionality of electronics along with reductions in both size, cost, and amount of power they use [3]. Distributed systems were made possible by the ongoing trend toward smaller, less expensive equipment and advancements in wireless communication [4]. These networks have the potential to be utilized for various purposes. Examples of potential applications include detecting hazardous chemical compounds in high-traffic areas and measuring tire acceleration and pressure [5, 6]. Various industry professionals believe that very low-wattage embedded electrical equipment will soon be an essential component of our day-to-day lives, performing various activities ranging from the automation of factories to our entertainment needs [7].

Despite this, the effectiveness of these emerging technologies is dependent on the accessibility of reliable sources of energy. Cost, size, and duration are issues for energy sources with fixed capacities, such as batteries. This research is based on energy harvesting, an alternative approach to addressing these challenges. The most recent iteration of structural health monitoring (SHM) systems incorporate low-power sensors and wireless communication components fueled by energy harvesters' outputs [8]. Energy can be extracted from the immediate environment to power autonomous sensor systems [9].

SHM integration into wind energy systems is a lucrative application for demonstrating SHM technology in general [10]. The components that must be inspected are large and difficult to inspect. During operation, wind turbines are subjected to intense and complex wind loadings; therefore, evaluating their dynamic responses to wind loads is desirable due to the possibility of fatigue and the desire to better comprehend the turbine's response [11]. In addition to fundamental condition assessment, monitoring may contribute to more efficient turbine operation. Wind energy harvesting has a limitation known as the "Betz Limit" (in practice, a multiplier of 0.593 (16/27) is applied to the maximum deliverable power), which is illustrated in Figure (1.1) as a maximum threshold for harvestable wind power.

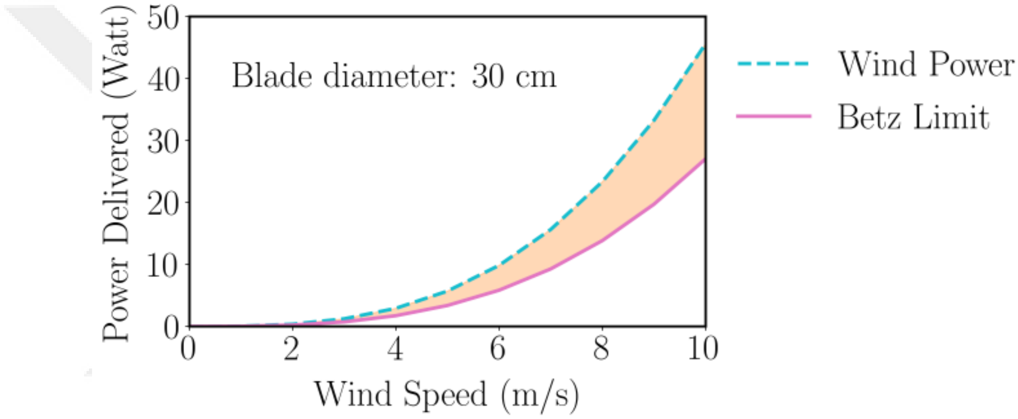

Figure 1.1: Betz Limit restricts the maximum wind power a fan propeller can deliver.

SHM can be performed with vibration-activated transducers because vibration is a common occurrence in nature. In recent years, there has been a great deal of interest in vibration energy harvesters employing piezoelectric transduction mechanisms due to their higher power density, ease of application, and scalability [12]. In situations with no fixed vibration, wind vibration powers piezoelectric harvesters. This thesis describes a piezoelectric energy harvester device dedicated to SHM in wind turbines by providing the necessary power for electronic devices through vibrational energy harvesting.

1.2 Energy Harvesting Phenomenon

In the 21st century, the method of energy harvesting has emerged as one of the most promising new fields of study and development. It refers to the collection of heat-losing energy from the environment. Differentiating energy harvesting from other renewable energy sources can be defined as collecting locally available natural energy for local use [13] . In most cases, it includes systems that have anything from nanowatts to hundreds of milliwatts of power. At these power levels, wireless devices make up the majority of the applications that are being used. Energy harvesting may or may not be applicable to certain devices depending on the kind and amount of energy available in the surrounding environment as well as the size limits. It has been proved, for instance, that the energy that may be harvested from body movements is often inadequate to power computers or cell phones, but that it is possible for a wide range of wireless sensors. When considering energy harvesting as a potential solution, it is also crucial to assess whether batteries, the most common kind of power source for wireless devices now in use, can match the criteria imposed by the particular application in question. There are many other possible sources of energy that may be collected such as motion and heat. There are three different transduction processes that may be used for the motion: piezoelectricity, electromagnetic induction, and electrostatic induction. In order to generate energy, harvesters make use of the Seebeck effect, light harvesters make use of the photoelectric effect, and chemical harvesters are able to make use of a wide range of chemical processes that take place on the surface of the electrode.

Energy harvesting, also known as energy scavenging, is the method of extracting energy from the environment and transforming it into usable forms, such as electricity. The energy may either be used right away or saved for use at a later time. The process of energy harvesting includes the collection of insignificant quantities of ambient energy that would be lost or left unused. It is yet too early to classify the process of energy harvesting as a fully evolved technological technique. It is not the solution to all of our energy problems. However, it has tremendous potential for powering low-power electronic devices.

1.3 Energy Harvesting Methods

Potential energy is being squandered all around us at any given time. Radio and Wi-Fi signals are continually surrounding us due to the abundance of electronic and mobile gadgets, for example. Our environment is rich in potentially usable energy that could power our electronic devices if captured and stored. Additionally, forms of lighting, heating, sound, or vibrations can all be examples of ambient energy representations. For instance, most power plants worldwide use turbines to transform thermal energy into mechanical energy [14]. The generation of electrical energy follows this. This process is highly inefficient, with over two-thirds of the energy input lost to the environment as heat and only one-third of the energy input converted into usable electricity [15]. Potentially, energy can be extracted from any of these sources, although not all are technologically feasible.

According to the type of energy source, there are a variety of energy harvesting technologies. In their most basic form, nevertheless, all energy harvesting systems are comprised of three primary elements: a source of energy; an interface circuit that draws the maximum energy possible from the sensor and converts it into a form that is appropriate for the application; a transducer that transforms the source's ambient energy to electricity; and a load, which may be comprised of electronic devices that make use of the energy that has been harvested [16].

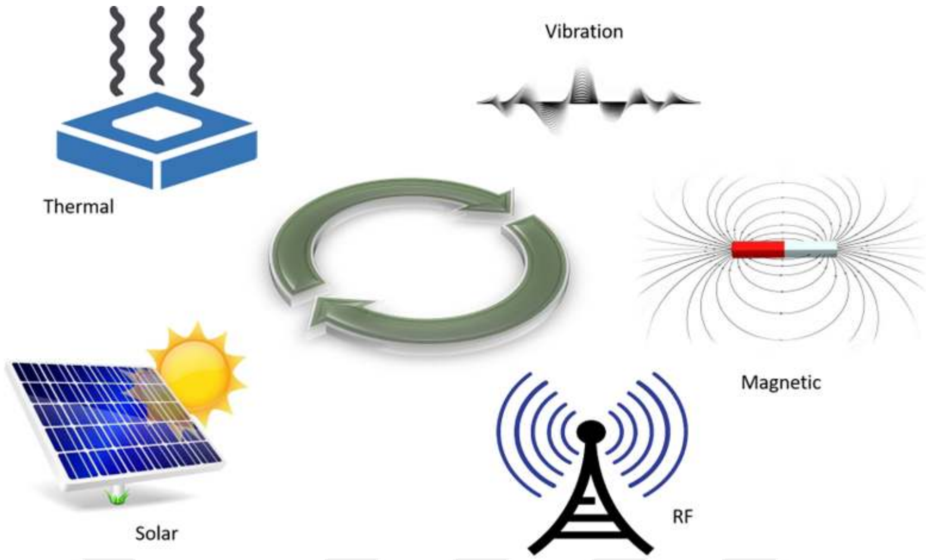

Figure 1.2: Widely used energy harvesting methods.

Photovoltaic cells are widely used to harvest solar energy. In order to convert light into energy in a straightforward manner, photovoltaic cells take advantage of a phenomenon known as the "photovoltaic effect." The creation of an electric current is the result of the photovoltaic effect, which is simply the act by which photons, the primary constituents of light energy, stimulate electrons to higher energy levels. Crystalline Si cells, thin-film cells, and junction cells are widely used PV cells. Solar cells are typically expensive. LEDs and photodiodes can be used instead of PV cells to harvest light energy and power low-power devices such as IoT devices. LEDs are relatively less expensive than photodiodes, but photodiodes provide more energy. Utilizing piezoelectric transducers, we harvest kinetic energy. Piezoelectric transducers convert the kinetic energy from vibrations, sounds, or motions into electricity. The transducer converts the kinetic energy into an ac source, and this current is then conditioned before being stored in either a thin-film cell or a supercapacitor. The vibration of a solid body can be induced by several variables, including uneven mass in a mechanism and structural wear and tear, and it can occur in practically all dynamical systems. Some of these factors include: Both the damping constant and the natural frequency are characteristics that can provide a concise description of the behavior of any individual system [17]. When researching the dynamic properties of a vibrating body linked with energy harvesting, it is common practice to use a lumped mass-spring system with one DOF [18]. The examination of the system's linear response is made more accessible by the fact that there is just one degree of freedom. The cantilever construction with a mass at the tip is the one that is used for piezoelectric energy harvesters the vast majority of the time.

Photovoltaic units and wind turbines are some most known energy harvesting devices. Micro integrated electronics rely on energy harvesting devices that gather milliwatts of energy from sources. Micropower energy harvesters may extend the life of batteries in retail, industrial, and healthcare applications where battery replacement is hard, costly, or impossible. Proper design can replace batteries with energy-harvesting devices.

Virtually every electrical system emits heat. This accounts for a significant portion of the energy that is lost. The Seebeck Effect is the name given to the phenomena in which a temperature gradient at the interface of two conductors generates electricity. The Seebeck Effect is the foundation upon which thermoelectric energy harvesting is built. This heat source might be something like a solar panel, a motor, or a water heater, to name a few possibilities. Temperature difference and TEG size directly affect energy output. Thermoelectric harvesting is used to supply wireless sensor nodes in industrial applications and other high-temperature locations, such as saunas. This allows the nodes to collect data without the need for batteries.

1.4 Energy Storage & Conversion in Sensor Nodes

Untethered sensor nodes improve mobility and deployment in inaccessible areas. Untethered nodes only function as long as their batteries live. Sensor nodes may employ low-power technologies, which reduces computing capability and transmission ranges. Several ways have been explored to enhance sensor node battery life. Energy harvesting is an alternate strategy utilized to alleviate the issue. Because a node will only be energy-constrained until the subsequent chance to harvest, the node's lifespan will be limited and will eventually end.

Depending on the energy consumption pattern of a node, techniques for energy harvesting have the capacity to satisfy all of a node's energy needs, or only a portion of those requirements. This is all dependent on how much energy the node consumes. The energy harvesting architecture comprises systems that capture and electrically transform ambient energy. The gathered energy can broadcast RFID signals, allowing the wearer to be tracked. Alternately, energy can be stored until sufficient quantities are collected for system operation.

Rechargeable batteries, prevalent energy storage, can be manufactured using various technologies. The technologies of sealed lead-acid, nickel-cadmium, nickel-metal hydride, and lithium-ion batteries are all considered to be superior [19]. The high output voltage, energy density, efficiency, and somewhat low self-discharge rate are characteristics of lithium batteries [19]. In place of or in addition to rechargeable batteries, supercapacitors can serve as storage components. They store charge but self-discharge at a significantly greater rate than batteries, up to 5.9% each day [20]. Their energy density is 5% of NiMH batteries, whose energy density is 100 Wh/kg. In contrast, supercapacitors have high charge-discharge efficiency and are immune to the memory effect [19]. This is particularly important if the node uses supercapacitors instead of batteries. RFIDs that store gathered energy for general-purpose computation constitute Computational RFID (CRFID). Solar energy is the kind of power that can be gathered at the lowest possible cost, in the shortest period of time, and with the fewest number of problems. Human power harvesting requires constant effort. CRFIDs typically have a one-second active life. By optimizing for both lifespan and performance, energy-harvesting sensor nodes can help designers tackle the problem of conflicting design goals.

To take advantage of these potential benefits, the node must predict the charge cycle's length, start time, and energy production. It must select and tune the parameters simultaneously to not use up all the energy available until the next recharging cycle. The architecture of sensor systems and solutions is directly influenced by the availability of harvesting opportunities, which make it possible to modify system characteristics and affect how solutions are implemented. To optimize energy balancing at the application level, it is necessary to fulfill all of the application's requirements at all times, provided that there is still using energy to gather. If energy isn't collected, the node won't work.

The ideal energy storage storage device device receives one hundred percent of the energy that is transferred from source to the storage and keeps the same amount of energy until it is used up. A realistic battery unit has a capacity that cannot be infinitely expanded, a charging efficiency that is lower than one hundred percent, and leakage that occurs even when there is no load. An energy harvesting architecture is presented by Kansal et al. for the purpose of estimating a node's sufficient power. A filter is used to energy usage and availability data collected over a certain number of epochs prior to the day of the acquisition, which is considered as if it were a single epoch. To achieve a more accurate estimation of the necessary amount of energy, Enhanced-EEHF makes use of the concept of rounds inside each cycle [21].

A mathematical model is proposed in [22, 23] to determine the optimal battery size and the rate of energy harvestability. In order to improve performance and reach energy neutrality at the node level, the model is utilized to adjust the duty cycle of each node where they are capable of using suitable energy estimates in order to pick and optimize parameter values on its own or in conjunction with other nodes. The method described in [23] uses a utilization metric taken from the application to compute the minimum and maximum duty cycles, and the duty cycle is modified dynamically to ensure that all gathered energy is optimally utilized. The quality of information supplied by a sensor is its sensing dependability. There is an exchange between the sensing reliability and the amount of energy consumed, much like there is with a node's pulse width and transmit power. Data aggregation and transmission can be carried out by nodes that capture energy. Nodes plan data distribution depending on estimated energy. When using nodes that are powered by solar energy, the quantity of energy that is accessible varies depending on the time of day. Harvesting nodes are responsible for primarily detecting and gathering data from adjacent to aggregate, storing the data, and performing other essential duties, as required, during the day. Energy harvesting adds a new layer to route selection: an awareness of energy efficiency. It is advantageous to have a higher proportion of energy harvesting units along the route to reduce end-to-end latency. This is because the duty cycle for every node on a route affects the delay experienced by the entire route.

1.5 Piezoelectric Energy Harvesters in Macro Scale

There have been reports in the research literature of energy harvesters on a macro scale. The piezoelectric energy harvester that Qian et. al. have developed is not only inexpensive but also bi-stable, making it completely unique. This energy harvester is designed to collect energy across a wide frequency range. The harvester is responsible for storing the potential energy induced due to the sub-beams mutual self-constraint and for harvesting the enormous amount of energy released during the quick shape shift. With a load resistance of 8.2 Ωk and an excitation frequency of 10 Hz, a power output of 0.193 mW may be harvested [24]. This is achieved using an amplitude of 4.0 g and a frequency of 10 Hz. The rapid shape change that occurs in the Venus flytrap's hyperbolic leaves served as motivation for the design of the energy harvester [24]. The double-leaf structure of the flytrap served as the primary source of inspiration for the design of the two sub-beams that are part of the biomimetic device that was designed using a cantilever beam as its base. The piezoelectric transducer is attached to the face of one of the sub-beams that is placed near to the clamped tip in order to capture the energy that is being generated [24]. The metal cantilever structure, composite macro fiber, and two rigid copper blocks were used to construct the bi-stable piezoelectricity harvester prototype. Full use is taken of the mutual constraint and equilibrium that exists between the two sub-beam constructions to realize the design's goals. There is a possibility that high-frequency vibrations will be limited to the beams as a consequence of the sudden release of energy that occurs during the motion that occurs between the two states. Increasing the frequency of the excitations has the potential to be of great use in the process of generating high power output; yet, this possibility has not been researched.

Experiments have shown that the system can be appropriately described by making use of the simplified model with a single degree of freedom, and the errors produced by this model are within acceptable limits. Even though it takes into account the nonlinearity of the beam, the model does not take into account the torsion that occurs. The natural frequencies that are present in the region, in conjunction with the stiffness that is found in close proximity to the steady state, may be used to calculate the harvester's effective mass . Bi-stable energy harvesting systems with deeper potential wells and more substantial barriers need more noticeable external excitations in order to trigger the proper snap-through dynamics [24]. This is because deeper wells hold more potential energy.

A sandwich structure, consisting of a layer with a soft core and two thin skins, can significantly lower the harvester's natural frequency while simultaneously increasing the voltage output [25]. Li et al. propose multiple single inner branches, each with a mass at its tip, connected to the primary substrate to produce multiple resonant spikes and tailor the frequency range of interest. Li et al. harvester produces a 2.48V, 6.21V, and 1.55V when examined at a low harmonic impulse of 0.02g [25]. These voltages are generated at three vibrational modes of 18.18Hz, 24.74Hz, and 28.12Hz, respectively [25]. In order to demonstrate the superiority of this design, a sandwich piezoelectric energy harvester that does not have multiple single inner branches has also been proposed. In order to get a low resonance frequency, the SPEH had to be coupled to a large tip mass [25].

When the power to total mass is a design limitation, such as harvesting energy from the motion of human limbs, a design such as this is not practicable [25]. The study presented a generic multi-branch sandwich piezoelectric energy harvester known as MSPEH [25]. The harvester has the capability of extracting energy from various sources of ambient vibration. It has a potential to provide power to electronics that are portable, as well as micro-electromechanical systems and wireless sensors. MSPEH provides numerous consecutive spikes of power or voltage output by using a repeated internal single branch, and the useable bandwidth and quantity of peaks may be changed practically by adjusting the multiple branches and the tip masses [25].

It has been suggested by Ramirez et al. that a novel piezoelectric energy harvester that operates at a light speed of rotation (0.5 to 3 Hz) could be developed [26]. The PEH is made up of a pair of E-shaped multiple beam systems that are connected by a single rigid beam. It may be adjusted in terms of the distance between its hubs and is installed on a solid plate that rotates at a fixed angular velocity. In addition to this, the angular speed does not change at all. The end goal of this strategy is to develop a mechanical design that has natural frequencies that are very low. This is accomplished by carefully selecting the diameters of the beam and the masses located at the harvester's tips, which allows for a greater degree of structural flexibility. This design features an additional E-shaped multiple-beam so that excessive displacements will not occur when an additional tip mass is added to the open end of the beam.

The highest electrical power output obtained from a PMN-PT single crystal measured by Song et al. was 1.07 mW at 89 Hz when the mass was 0.53 g [27]. Karami et al. investigated how well single-crystal PMN-PZT and commercial PZT-based materials performed compared to unimorph cantilever energy harvesters. They discovered that the piezoelectric energy harvester made with a single crystal delivers a higher power output when compared to the piezoelectric ceramics made with many crystals. Compared to polycrystalline ceramics, the power output produced by single-crystal piezoelectric materials such as PMN-PT and PZT-5A was significantly higher. The cantilever-type energy harvester had a maximum output of 226 W/g^2 at 819 Hz [28], whereas the single crystal had a maximum power output of 1.07 mW at 89 Hz under 0.53 g [29]. There was a wide range of natural frequencies displayed by three cantilevers of varying lengths, and there was a 5.4 percent frequency bandwidth with a 3dB attenuation. Under 1 g, the maximum power production was measured at 32 Watts at 1100–1165 Hertz [29]. These data show that altering the cantilever's length changes the natural frequency by tuning. While the hub is turning, a gravitational force causes mechanical vibration energy to be exerted on the PZT cantilevers of this structure. The rotation of the hub causes this energy. At an angular velocity of 21.96 Hz, they obtained the maximum power of 6.4 mW [30]. The off-resonance behavior of the piezoelectric generator, in conjunction with its high-power output, makes it possible to accomplish more practical ways of using the device. Diaphragm structures from other researchers [31] and other similar structures would be crucial for high-performance and practical applications.

Li et al. proposed a new sandwiched harvester design in their work. The substrate structure comprises two layers of metal on either side of a layer of flexible material in the center. When both the geometrical dimensions and the tip mass of the CPEH and the SPEH are held constant, the SPEH will produce 18.8 percent more output voltages at resonance than the CPEH [32]. A unique piezoelectric energy harvester is described in the SPEH publication. The harvester has two metal sheets and a soft base. The linear small deformation assumption is used to describe each layer's elastic behavior dependent on the substrate. Because the sandwiched substrate and layers are both thin, it is possible to ignore the typical stress applied in the thick direction. At resonance, SPEH produces a voltage output that is 18.8 percent higher and generates 130.8 microwatts, 426.6 microwatts, and 1158.0 microwatts, respectively, at base accelerations [32].

Because of its enormous potential to replace batteries in WSN and low-power-consuming autonomous electrical items, energy harvesting from vibrations utilizing piezoelectric materials has attracted much attention from researchers [33]. The proposed harvester by Upadrashta et al. has the capability of being engineered to function within the frequency band of the vibration source of interest. The construction consists of a core cantilever with a macro-fiber composite patch attached to it and three branches with tip masses linked to the main beam's open end. The main cantilever beam of the MPEH harvester has a patch of macro-fiber composite attached to its surface. The open end of the primary cantilever beam has three branching beams linked to it, each of which has a mass at its tip. Because the MPEH's shape is similar to that of a three-pronged spear, it is referred to as a trident-shaped MPEH. In order to obtain closely spaced resonant peaks, it is necessary to select the structure sizes using parametric analyses. When tested with a harmonic stimulation of 0.2 g_{RMS}, the harvester produces 3738 µW, 47 µW, and 123 µW at its three resonant peaks [33]. The mentioned harvesters are visually shown in Figure (1.3a-e.).

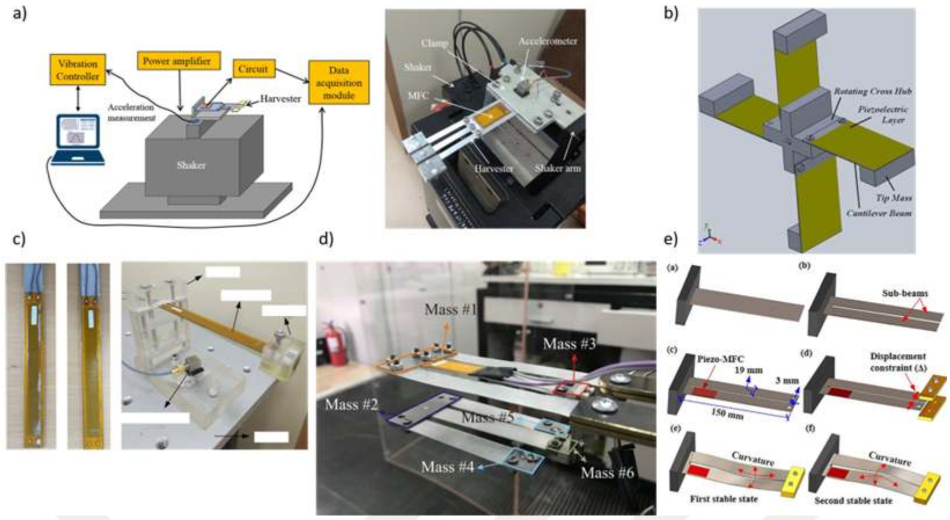

Figure 1.3: a) The device was engineered to function within the frequency band of the vibration source of interest [33] b) A gravitational force causes mechanical vibration energy to be exerted on the PZT cantilevers of this structure [31] c) The substrate structure comprises two layers of metal on either side of a layer of flexible material in the center [32] d) A novel piezoelectric energy harvester that operates at a light speed of rotation by Ramirez et al. [26] e)The rapid shape transformation of the Venus flytrap's hyperbolic leaves served as inspiration for the energy harvester's design [24].

In Rui et al. research, a magnetically coupled piezoelectric energy harvester is presented. Its purpose is to boost the output and bandwidth of a test platform constructed using the Macro Fiber Composite material. The system can reach its max output power of 35.0 mW while achieving a maximum electrical power of 3.28 mW when subjected to excitations of 4 m/s^2 [34]. The performance has been exceptional compared to the traditional single cantilever beam—magnetic coupling results in an increase in both the amplitudes and bandwidth of the signal. The amount of energy that is used by a wireless sensor system may be as low as mW or even µW at its lowest point. A bimorph design can be exploited to produce more energy, which can be crucial in situations where the required amount of energy is insufficient. The power output of the PZT can be enhanced by approximately 35.0 percent if the cantilever beam's magnetic deviation and the system's size and volume are both increased by approximately 100%, respectively [34]. Since piezoelectric materials are the primary cost source, it is anticipated that the overall cost will increase by less than twenty percent [34].

Researchers have shown a diaphragm device that can collect energy from repeated pressure patterns or periodic acoustic waves [35, 36] in addition to mechanical vibrations. This is because the diaphragm is a very adaptable construction. In PEH architecture, layer poling orientations align with pressure. This allows for the utilization of the d_{33} mode that has a higher coefficient than the d_{31} mode [37].

Using piezoelectric generators is one method that can be utilized to extract energy from roadways and railways. In the 1960s, the idea of using mesoscale PEHs to provide power for pacemakers was one of the earliest to be considered. Hasler and colleagues developed an implanted energy harvester in 1984 with the purpose of power generation from the movement of ribs that occurs during respiration [38]. In 1996, Umeda et al. were the ones who came up with the idea of using PEHs to charge the batteries of portable electronic gadgets [39]. In that work, power conditioning circuitry that was both efficient and effective was used to correct the output and store the resulting charge on a capacitor. Shenck et al. proposed an energy harvester which at a walking pace of 0.8 hertz, generated a continuous power output of 1.3 milliwatts [40]. Fabrication and testing of a cantilever-type vibrational mode PEH by Glynne-Jones and colleagues were published in 2001 [41]. The proposed device was tapered with and had two electrodes. The piezoelectric layer was attached to a 23-millimeter steel beam. At 0.8 mm tip displacement, it had an 80 Hz resonance frequency and generated 3 µW at 333 kΩ [40].

It has been established in several experiments that the structure of a diaphragm can also be used to capture vibrational energy. This construction has a rigidity that is significantly higher than that of a cantilever of the same size, resulting in a 1.71 kHz resonance frequency [42]. A 29mm diameter, 1mm thick cymbal shaped harvester with 7.8N at 100 Hz produced 39 mW. [43].

Investigations into the practicability and dependability of large-scale PEHs are now being placed. The deployment of such systems would necessitate significant financial investments; hence, commercialization of these technologies can only be anticipated if it can be demonstrated that they are feasible. In research, in order to harvest vibrational energy, a PZT energy harvester with 300 layers was used.

In resonance mode, the stack generated 15 mW at 1767 Hz, and in reaction to a 1 N_{RMS} force, it created 15 µW at 800 Hz [44]. In Cao et al. research, millimeter-scale generators were created by depositing AlN thin films on stainless steel, and then the vibrational energy harvesting performance of these generators was measured. In general, single crystal silicon is utilized as the substrate for piezoelectric thin films because it is simple to produce, is chemically stable at high temperatures, and does not have an exceptionally high price tag [45]. If cooperation with microfabrication technologies is not necessary, then using stainless steel as the substrate for piezoelectric thin films to fabricate small generators with a low resonance frequency is a good idea. Electroplating is a method that can produce copper and nickel, but the low yield strengths of both metals imply that they have poor stiffness when compared to one another. It is also anticipated that the materials chosen will have high mechanical strength, measured by factors like fracture strength and toughness.

AlN material play a role in the creation of micro piezoelectric generators throughout the production process. ZnO may have a greater k_{31}, but in general, it has a vast dielectric loss. In a research involving macro-scale energy harvesters, the ideal aspect ratio was less than 0.4, and the ideal thickness ratio was 3.1 for an AlN-stainless steel structure [45].

Mehraan et al. describe a tapered cantilever beam design showing that the power output of the PZT can be enhanced by approximately 35.0 percent if the cantilever beam's magnetic deviation and the system's size and volume are both increased by approximately 100%, respectively [46]. Because piezoelectric materials are the primary cost source, it is anticipated that the overall cost will increase by less than twenty percent. As a result of the fact that the material functions as a current source when prolonged vibration is present, the amplitude of the current is reliant on the intensity of the vibration.When a clamped capacitor is charged using a series of voltage increments, the resistance to the energy flowing out from the clamped capacitor is reduced. Also, in [2], a comparison is made between the rectangular and trapezoidal cantilever beam geometries, as well as their respective strain profiles by Roundy et al. Considering the most significant amount of strain that the material can tolerate at each point along the tapered beam is required in order to produce the uniform distribution of strain that is necessary to obtain the maximum average strain.

It is proposed by Becker et al. that a novel form of piezoelectric energy harvester with an auxiliary synchronized switching interface might be used to maximize the efficiency of power transmission from an energy harvester to a storage component [47]. The system has been improved by adding a novel interface circuitry based on the first energy injection proposed by Lallart et al. [48]. It makes possible a process of energy harvesting almost independent of the load and a process of energy storage almost optimal. The mechanism might be three times as efficient as traditional ones, according to the study. The generator can be separated into two distinct elements, one of which is used for the primary harvester and the other to provide energy bursts for the harvesting algorithm [47]. Both of these structures are used in the harvesting process. The mentioned harvesters are visually shown in Figure (1.4a-c.).

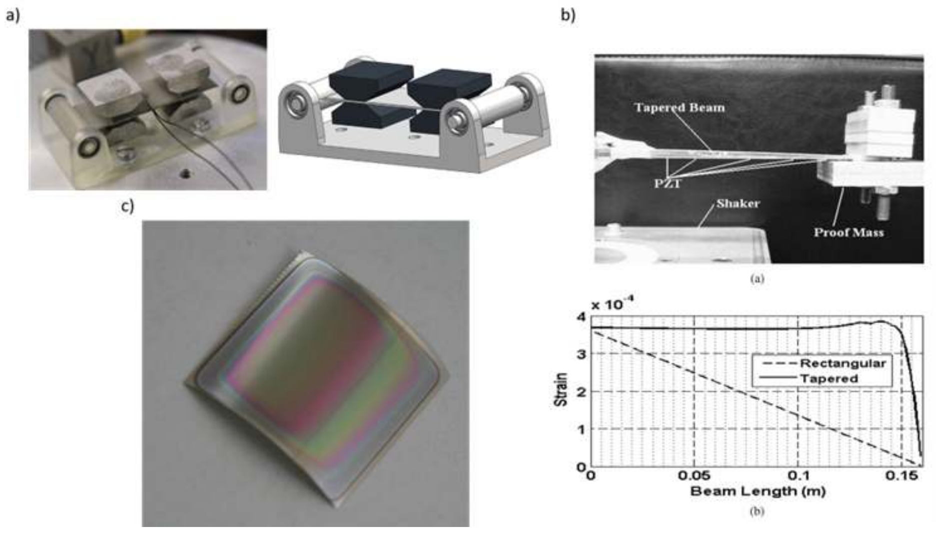

Figure 1.4: a) The generator can be separated into two distinct elements, one of which is used for the primary harvester and the other to provide energy bursts for the harvesting algorithm [47] b) A tapered cantilever beam design showing that the power output of the PZT can be enhanced by approximately 35.0 percent described by Mehraan et al. [46] c) Millimeter-scale generators were created by depositing AlN thin films on stainless steel [45].

Clamped cantilever beams have a mass placed at one end of the beam and another mass fastened at the other side of the beam. A four-point bending principle was used in the design that was given in this research in order to ensure that the stress was distributed evenly throughout the structure. The fundamental idea behind the first energy injection method is to harvest the energy from the piezoelectric material whenever the output voltage reaches its maximum level [48]. The four-point bending approach leads to optimal power output due to a homogeneous stress distribution across the entire structure. Mechanical energy harvesting and electrical connection operations must be addressed to define interface circuit parameters and switch strategies. This can be accomplished by combining the two sets of information. For these simulations, mathematical SPICE-based simulation tools could be utilized in the research. Table (1.1). compares the macro scale harvesters proposed in the section.

Table 1.1: Macro Scale Harvester Parameters Compared.

Paper	Dimensions	Shape	Voltage Output	Power Output	Resonance
[24]	150x19x3 mm^3	Venus flytrap	Reported in figures	0.193 mW	12.47 Hz
[26]	Between 85 to 150 mm	Linked E-shape	6 V max.	200 μW	4.7 Hz
[27]	105x12x1.6 mm	Unimorph cantilever	∼19 V	1.07 mW	89.80 Hz max.
[30]	50.8×38.1× 0.13 mm	Rotary	Reported in figures	Reported in figures	21.96 Hz
[32]	100×10x1.5 mm^3	Sandwich	16.6 V with tip mass	1158.0 μW at 0.2g	30 Hz
[33]	50x26x1 mm^3	Trident- shaped	$7.4V_{rms}$	3738 μW max.	15-20 Hz
[34]	63.6 [cm^3]	Magnetic coupled	19.83 V	3.28 mW	15.3 Hz
[38]	2.6x40 mm^2	Stretchable	18 V	∼20 μW	Not given
[40]	5x5 cm^2	Shoe- mounted	5-6 V	1.3 mW	Not given
[41]	23x23 mm^2	Cantilever	Reported in figures	3 μW	80.1 Hz
[42]	25 mm diameter	Circular membrane	Up to 3 V	0.65 mW	1.71 kHz
[43]	29x1 mm^2	Cymbal	Reported in figures	39 mW	Not given
[44]	32.4x7.6x7.1 mm^3	Multilayer stack	4.7 V_{RMS}	414 mW	1204 Hz
[45]	Reported in figures	Rectangular	2.10 V	5.130 μW	69.8 Hz
[46]	13x1x0.4 cm^3	Tapered beam	100 V	5 mW	Not given
[47]	31.8x10x 0.38 mm^3	Four-point-bending	∼3 V	Not given	Not given

1.6 Piezoelectric Energy Harvesters in Micro Scale

The performance of vibrational energy harvesters, in contrast to that of electronic circuits, is substantially or primarily dependent on the dimensions of the harvesters. Unimorph MEMS PEHs have a lower electromechanical conversion factor than bimorphs. Reducing the resonance frequencies of sub-mm length cantilevers below 250 Hz is challenging due to their small weights and comparatively high spring constants. This is primarily due to the cantilever's short dimensions, which, in turn, produce a high cantilever rigidity and a low cantilever mass. It is feasible to lower this resonance frequency by utilizing thick, robust mass layers [38].

Morimoto et al. discovered a 2.8-micron-thick piezoelectric film mounted to a 50-μm cantilever could produce 244 milliwatts of electricity at 126 Hz without structural damage with PZT sensor having a stainless steel structural layer [49]. Aluminum nitride (AlN) is a piezoelectric material frequently employed in energy harvesters. Even though it has a smaller electromechanical coupling coefficient than PZT, it is still a popular choice. Sputtering is a simple method for depositing AlN, which is one reason it is considered a potential alternative for CMOS-compatible PEHs. Most MEMS size PEHs are cantilever form devices that collect vibrational energy from their surroundings. There have also been reports of energy harvesters that operate under pressure. These energy harvesters can extract energy from pressure variations in the operating medium. A diaphragm-type PEH was successfully manufactured in 2006, and its output power was measured to be 0.34 µW/cm^2 at a sound pressure level of 149 dB [50]. This design is similar to the design proposed in this thesis for utilizing circular features. Figure (1.5) shows the 3D image of the piezoelectric element proposed in the thesis. It is possible to cultivate ZnO nanowire nanostructures made of flexible substrates, which may be crucial for the development of implantable energy harvesters. When activated by an ultrasonic pulse, one of the devices that were manufactured produced a DC power output of 1 pW from an active region that was 2 mm^2 in size [51]. The same group of researchers showed wireless self-powered device [52] and a sensor that draws power from a wheel that is continuously turning and demonstrating their potential use as a pressure sensor

[53, 54]. PZT and AlN are the two piezoelectric materials most commonly favored for use in cantilever-type PEHs.

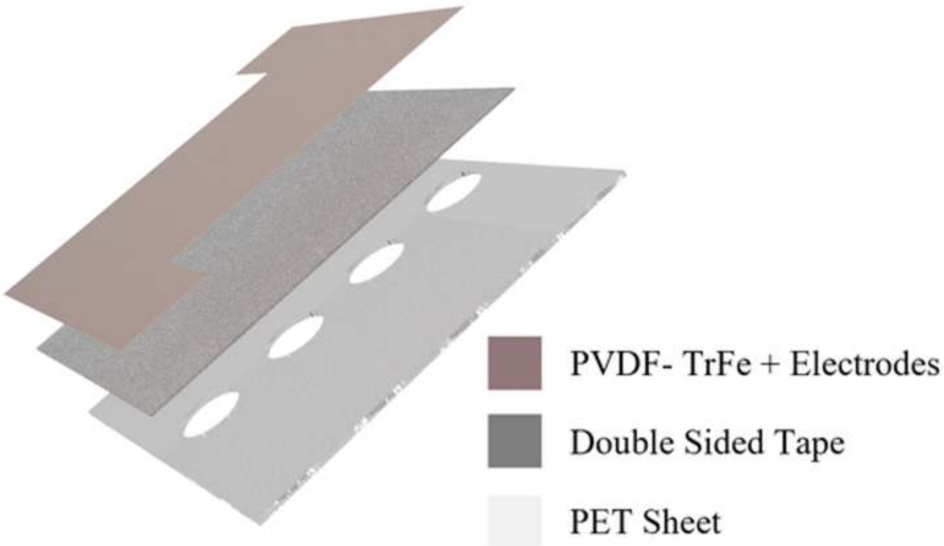

Figure 1.5: The sensor is built on 3 main layers.

The concept of a brand new wireless self-powered sensing microsystem has been proposed and prototyped by Tang et al. [55]. The microsystem can assess the amplitude of disturbing vibration independently. It can wirelessly broadcast a warning and notification signals when it meets the required threshold. The event-driven sensing and warning function is made feasible by utilizing a piezoelectric energy harvester. This harvester does not begin to create electric power until the monitored vibration level hits a critical threshold. The signal for alarming and notifying can be exceedingly straightforward, such as a code that indicates the occurrence location in the case of oil pipeline theft alarming. A warning signal should be sent out whenever the motion of an impact hammer or grinder becomes so intense that it poses a risk to the operator's health.

In the testing scenario proposed by Tang et al., the stage that generates power begins to vibrate freely at its resonance frequency to produce electrical power. They wanted to measure if the magnitude of the incoming vibration was high enough and if it was possible to perform enough work to counteract the force and activate the power-generating stage. The simulated hysteresis of the force applied in the article shows that a part of the energy is transmitted from the sensing stage to the producing stage with each cycle. The gap distance between the two stages plays a role in determining the maximum force as well as the location of the edge. The mentioned harvesters are visually shown in Figure (1.6a-d.).

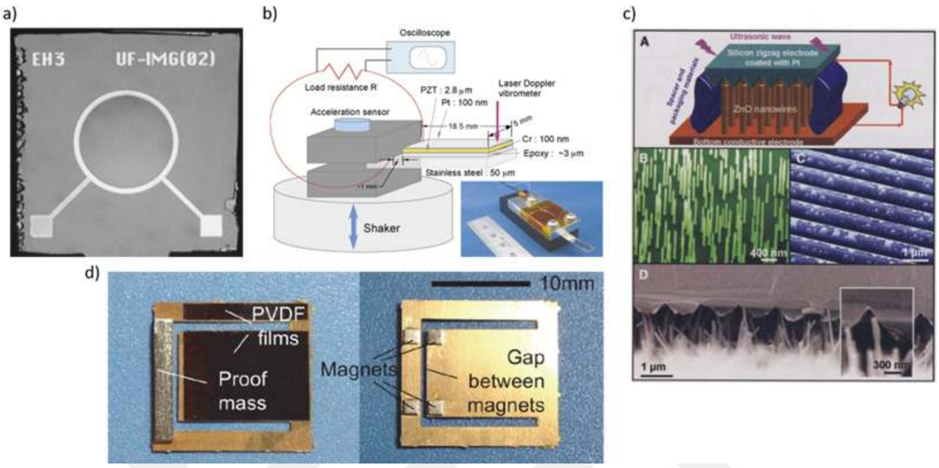

Figure 1.6: a) Diaphragm-type PEH with an output power of 0.34 µW/cm^2 at a sound pressure level of 149 dB [50] b) A 50-micron-thick steel cantilever could provide 244 milliwatts of power output at 126 hertz when subjected to an acceleration of 50 meters per second square [49] c) The device produced a DC power output of 1 pW from an active region that was 2 mm^2 in size [51] d) The harvester does not begin to create electric power until the monitored vibration level hits a critical threshold. The signal for alarming and notifying can be exceedingly straightforward, such as a code that indicates the occurrence location in the case of oil pipeline theft alarming [55].

Voltage thresholds typically range from 1g to 6g, and they are prevalent in applications such as monitoring vibrations caused by power tools for worker safety [56]. When the device is being pushed through an acceleration that gets higher than the critical, the device's voltage will always be significantly higher than the output below the threshold. This vibration-based triggered energy-generating technology may be expanded to other situations where the vibration is considerably weaker if further optimization is performed, for as by weakening the magnets or placing the two vibrating stages into a configuration that is not coplanar. When a host structure is damaged in some way, its resonant modes get activated, and it is necessary to consider these eigenfrequencies. The increasing gradient of the stimulated generation can determine how sensitive a harvester is when it is aroused by vibration and the acceleration is close to the threshold.

The findings of Tang et al. make it abundantly evident that the gadgets create a significant amount of electricity when triggered by vibration. Each sort of harvester has attained a rise in energy greater than eight times the previous level. The form of the bistable component ensures excellent sensitivity, which features a steeply increasing slope close to the threshold. The electric power produced can either be provided to a simplified radio-frequency front-end to broadcast the vibration monitoring signal, or it can directly drive an alarm.

Because of the need for batteryless implants, lead-free materials for piezoelectric nanoscale and micro generators have gained popularity. In Gupta et al., the flexible device demonstrates exceptional performance with a vast output voltage of 48 V and output current density of 0.43 A/cm^2 under vertical compressive stress of 2 kgf [57]. This enabled an energy conversion efficiency of approximately 11 percent to be attained [57].

On a Silicon on Insulator substrate, a CMOS-compatible technique that involves Aluminum Nitride thin films was created by Defosseux et. al. Under complete vacuum conditions, the captured energy hits the same level but weighs only 0.15 g [58]. The conclusion drawn from this finding is that enclosing piezoelectric energy harvesters in a vacuum-sealed container is a highly intriguing approach.

The Deterre et al. device has the potential to evolve into a miniature, long-lasting energy source that can power active implanted medical devices like leadless pacemakers [59]. It makes it possible to harvest direct readings of blood pressure and makes it possible to transfer energy with high efficiency. At a frequency of 1.5 Hz, the best designs have achieved a power of 3 J/cm^3/heartbeat and a transduction performance of 5.7x10^{-3} [59]. It is predicted that this power could be increased by a factor of two by employing the same design process and material [59]. A geometry that is long and thin makes it possible to reduce the stiffness.

Deterre et al. employ a flexible transducer to increase mechanical energy input. Because metals are stiff, metal packaging must be engineered to be flexible. In [60], a spiral was used, but it wasn't coated by electrodes and didn't create electricity.

Fabrication issues and the depth of charge dispersion on spirals lead to intricate electrode designs. Using this technology, 10 m-thick electrodeposited nickel micro-bellows have been created. The model was tested by applying a load to its top surface's center. Its 140 N/m rigidity is impressive given its size and substance. In each situation, the input force peak amplitude is 180 mN of the proper electrode pattern. [59].

The decrease in efficiency is primarily attributable to the wasteful rising number of arms, which occurs as the spirals get more compliant. Finding a medium between the output power and the authorized displacement will be necessary when deciding on a spiral design. Work has been done to optimize the electrode size using FEM simulations. In light of these findings, they concluded that the negative group of electrodes contributes very little to the overall power. This design's output energy density per loop is not noticeably superior to standard inertial energy harvesters in the literature. There were a few different enhancements that could be implemented in order to boost the amount of energy produced. If higher-performance materials were used, such as monocrystals, which have been shown to give superior coupling and can be supplied in a thinner form, the requirement for a curved arm would be reduced [59].

In addition to biocompatibility and hermeticity, flexible packaging introduces durability and tissue development protection. It's more miniaturized than an energy harvester, whose volume can't be lowered while retaining a low resonance frequency. One possible alternative would be to use palladium or some other biocompatible metal capable of being electrodeposited in place of nickel [59].

In Leland et al. research, the free end of the sensor is fitted with a microscale permanent magnet affixed to a piezoelectric MEMS cantilever [61]. When a magnet is introduced near an AC wire, it couples to the wire's pulsating magnetic field. This bends the cantilever and provides sinusoidal voltage proportional to current. This sensor can measure current in a two-wire "zip-cord" without encircling the conductor, unlike inductive sensors. Self-powered, it's better for wireless sensor node applications than a driven sensor [61]. Its ends had neodymium magnets.

Leland et al. devices could function at various intervals without needing a battery, thanks to the harvested power source. A regulator made by Microchip Technologies called the MCP1801T and an inverter made by Maxim called the MAX828 were used to amplify the sensor signal [61]. An alternating current MEMS sensor was created by affixing a microscale permanent magnet to the free end of a piezoelectric aluminum nitride MEMS cantilever. This allowed the sensor to detect the alternating current. This cantilever was utilized in the production of a MEMS sensor. When the sensor is put nearby, it displays linear response and can measure the amount of alternating current (AC) flowing through single wires and two-wire zip cables. It has been proved that it is possible to create a self-powered integrated sensor module by employing an energy harvester to power the signal conditioning circuitry of the sensor at a duty cycle of 2.6 percent [61]. The mentioned harvesters are visually shown in Figure (1.7a-d.).

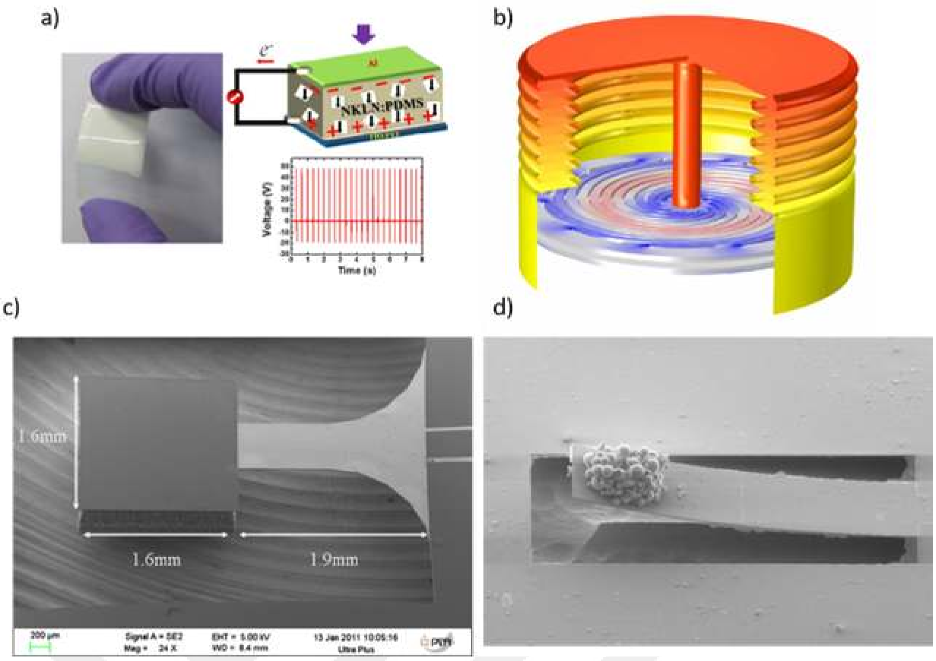

Figure 1.7: a) The flexible device demonstrates exceptional performance with a vast output voltage of 48 V and output current density of 0.43 A/cm^2 under vertical compressive stress of 2 kgf [57] b) The device makes it possible to harvest direct readings of blood pressure. It makes it possible to transfer energy with high efficiency to a transducer that operates in a quasi-static mode [59] c) Under complete vacuum conditions, the captured energy weighs only 0.15 g [60] d) An alternating current MEMS sensor was created by affixing a microscale permanent magnet to the free end of a piezoelectric aluminum nitride MEMS cantilever. This allowed the sensor to detect the alternating current [61].

In Cui et al., a unique piezoelectric cantilever with multiple beams has been developed to harvest energy from vibrations. Imaging with an atomic force microscope (AFM) and X-ray diffraction (XRD) was used to measure the properties of the PZT ($Pb(Zr_{0.53}Ti_{0.47})O_3$) thin layer. Under conditions with an acceleration of 1g and a frequency of 260 Hz, the multi-beam has the potential to achieve an output voltage of 80.78 mV [62]. The voltage applied is 2 mV, the frequency ranges from 100 to 700 hertz, and the acceleration is 9.8 meters per second squared [62]. The voltage output rises as the vibration acceleration rises. Both of these trends are consistent with one another. When the load resistor was 50 Ωk and the power reached its maximum of 20 mV, the load produced a voltage of 16.6 mV [62].

In Tang et al. article, a microcantilever constructed using MEMS technology was proposed. This microcantilever is based on the bonding of a bulk PZT wafer and phosphor bronze, and it is created using mechanical chemical thinning and etching [63]. This fabricated design has an open-circuit voltage output of 35 volts, a power output of 321 microwatts, and a power density of 8664 microwatts per cubic centimeter, and these values are measured at the resonant frequency of 100.8 hertz [63]. When it matches an optimal loading resistance of 140 Ωk under the stimulation of 3.0g acceleration, this fabricated prototype has an output power of 8664 microwatts per cubic centimeter [63]. It recovers vacuum pump vibration efficiently. It has been determined that the micro-generator that was manufactured has an adequate volume of 0.03732 cm^3 Moreover, its acceleration has grown from 0.5 g to 3.0 g. Additionally, the power density has increased by 24.7 times, going from 351.02 W/ cm^3 to 8664 W/cm^3 [63]. Compared to other 10 Hz to 300 Hz devices, this one has excellent output under high acceleration [63].

Phosphor bronze and bulk PZT both have room for further reduction in their thickness, which would allow for overall dimension reduction and an increase in output power density [63]. Because of the vacuum pump's high vibration level, Tang et al. micro-generator working on it could light up one of the light-emitting diode (LED) bulbs. When the acceleration of the vibration increases, it causes the chargeable voltage to rise while simultaneously reducing the required time. In the article, some power-efficient electronics were designed to operate for extended periods without needing to be recharged. This configuration combined a tungsten-proof mass with a cantilever beam made of phosphor bronze and a piezoelectric wafer to achieve a resonance frequency of 105 Hz or lower [63]. The component can withstand a vibration acceleration of 7.0 g and produce an output voltage of 61.2 V [63].

In Purusothaman et al., it has been shown that antimony sulfoiodide, also known as SbSI, can function as an efficient energy harvester due to the ferroelectric-semiconductor properties it possesses [64]. They investigated whether or not it would be possible to develop SbSI-based piezoelectric nanogenerators using polymer matrix interfaces, such as polydimethylsiloxane, polyvinylidene fluoride, and polymethylmethacrylate [65]. Lattice vibrational modes of less than 400 cm^{-1} are displayed by SbSI. These modes can be separated into two distinct frequency ranges: the low-frequency range and the high-frequency range [65]. Table (1.2) shows the comparison of the micro-scale harvesters proposed in the section.

Table 1.2: Micro Scale Harvester Parameters Compared.

Paper	Dimensions	Shape	Voltage Output	Power Output	Resonance
[49]	18.5x5 mm^2	Cantilever	2.6 V	244 μW	126 Hz
[50]	Reported in figures	Circular diaphragm	4.6 mV	0.34 $\mu W/cm^2$	3.7 kHz
[51]	$\sim$2 mm^2	Nanowire	Reported in figures	Reported in figures	$\sim$3 MHz
[52]	1.5$\times$0.5 cm^2	Nanowire	1.5 V	70 $\mu W/cm^3$ power density	Not given
[54]	500 nm x 6 μm	Nanowire	8V	$\sim$5.3 mW/cm^3 power density	Not given
[57]	2 $\times$ 3 cm^2	Microcube	48 V	Not given	Not given
[58]	2.8 mm^3	Cantilever	89 mV	0.62 μW	214 Hz
[59]	21 mm^3 volume	Micro-bellows	Not given	Reported in figures	Heartbeat
[60]	1.2 cm^3	Spiral bimorph	Given in figures	3.25 μW	10 Hz
[61]	1000 $\times$ 200 μm^2	Cantilever	Given in figures	Not given	60 Hz
[62]	2600$\times$760$\times$20 μm^3 [63]	Multi-beam	20 mV	Not given	Not given
[63]	As given in a table [64]	Rectangular beam	61.2 V	321 μW	100.8 Hz
[64]	0.5x0.5 cm^2	Tubular	Given in figures	4.6 $\mu W/m^2$	100.8 Hz

1.7 Objectives

The proposed device is intended to cater to the requirements imposed by energy harvesters. Because of its simplistic design, it is easy to implement using conventional methods, which enables the production of sensors of a comparatively compact size. The equipment in question needs to be examined to provide evidence supporting these statements. As a result, this study aims to accomplish two things: first, it will present and compare different techniques of analysis of the proposed device, and second, it will determine whether or not the suggested device is a viable choice for energy harvesting for SHM in wind turbines.

1.8 Organization

The following is a list of all eight chapters that make up this report. The first chapter overviews several piezoelectric energy harvester designs that can be scaled to various sizes. The governing physics of transduction and piezoelectricity are discussed in Chapter 2. These topics are then used to show the one-dimensional analysis of transducers using a lumped-parameter circuit and finite element models in COMSOL® Multiphysics. Chapter 3 presents extensive information about piezoelectric materials and a comparison of these materials to one another in addition of several experimental PVDF-TrFe characterizations and many stages of the harvester's construction. The testing phase is described in Chapter 4, and the outcomes of these examinations are discussed in Chapter 5 with an overall summary in Chapter 6.

Chapter 2

MODELING OF THE PIEZOELECTRIC TRANSDUCER

2.1 Mathematical Modeling

In the electrical domain, there is a capacitor, and in the mechanical domain, there are spring and mass elements. Ideal transformer elements are used to indicate domain coupling. The mechanical domain damping caused by anchor loss and other factors is insignificant; hence it is not considered in the model. Table (2.1) contains the model parameters.

Table 2.1: Values for Equivalent Circuit of PEH.

Symbol	Description	Unit [SI]
C	Electrical Capacitance	F
r_{pm}	PVDF thickness	m
I_m,I_e	Piezoelectric coupling integral, Strain energy integral	-
M	Piezoelectric bending moment	CVs^2/kg
$e_{31,f}$	Transverse piezoelectric coefficient	C/N
V_{in}	Applied voltage	V
z	Neutral plane	m
t_k, z_k, E_k	Layer thickness, the center axis, Young modulus	m,m,Pa
v_k	Poisson's ratio	-
D,h_k	Flexural rigidity, distance to layer surface	Pam^4,m
μ_{eff}, ρ_k	Effective mass per unit area, density	-
k_m	Stiffness	kg/s^2
η	Electromechanical coupling	Cm/N
f_n	Resonance frequency	Hz

λ_{01}	The eigenvalue for the first mode vibration	-
m_d,m_m	Total mass, Modal mass	kg

The capacitance, C, is described in the electrical domain as a conventional parallel plate capacitor having capacitance defined by [66]:

$$C = \varepsilon \pi {r_{pm}}^2 / t_{pvdf}. \tag{2.1}$$

where ε represents the proportion of relative permittivity of PVDF to the permittivity of a vacuum, t_{pvdf} represents the PVDF thickness, and r_{pm} represents the radius of the top electrode. This radius, r_{pm} = r x is a portion of the plate's radius. In this case, r_{pm}=r. With a normal plate deflection shape function of φ(x) a clamped model has been assumed [67]:

$$\varphi(x) = (1 - {x_\theta}^2)^2 \tag{2.2}$$

where x_θ is the radial coordinate in its normalized form. The axisymmetric plate deflection is w(x_θ)=$w_0\varphi$(x), where w_0 is the static deflection at the clamped plate's center. One can calculate I_m, piezoelectric coupling integral and I_e, strain energy integral by which are specified as [66]:

$$I_m = 1/(1 - v) \int_0^\gamma ((x_\theta d^2\varphi(x_\theta)/d{x_\theta}^2) + (d\varphi(x_\theta)/dx_\theta))dx_\theta \tag{2.3}$$

$$I_e = \int_0^1 ((x_\theta d^2\varphi(x_\theta)/d{x_\theta}^2)^2 + 2v(d\varphi(x_\theta)/x_\theta dx_\theta)(d^2\varphi(x_\theta)/d{x_\theta}^2) + (d\varphi(x_\theta)/dx_\theta))dx_\theta \tag{2.4}$$

where v is the composite plate's effective Poisson's ratio, and M is the piezoelectric bending moment provided by [68]:

$$M = -e_{31,f} V_{in} z \tag{2.5}$$

The transverse piezoelectric coefficient is $e_{31,f}$. The applied voltage is V_{in}. The distance between the active PVDF layer's mid-plane and the neutral plane is z. It is worth noting that the piezoelectric coupling integral I_m is computed solely over the electrode region, but the strain energy integral I_e is computed across the whole radius. The location of the composite plate structure's neutral plane z is defined by:

$$z = \sum_{k=1}^{3} (t_k z_k E_k/1 - v_k^2) / \sum_{k=1}^{3} (t_k E_k/1 - v_k^2) \tag{2.6}$$

Counting from the bottom, the subscripts denote the thin plate layers. The Youngs modulus is E_k the Poisson's ratio is v_k and the center axis of each layer is z_k. Similarly, the composite plate's flexural rigidity, D [69], and effective mass per unit area, μ_{eff}:

$$D = \sum_{k=1}^{3} 1/3((h_k - z)^3 - (h_{k-1} - z)^3)/(1 - {v_k}^2/E_k) \tag{2.7}$$

$$\mu_{eff} = (1/D) \sum_{k=1}^{3} \rho_k t_k \tag{2.8}$$

ρ_k is the density and h_k is the distance to the top of each layer. One gets when solving (11) for the mechanical compliance $1/k_m$:

$$1/k_m = r^2/2\pi D I_e \tag{2.9}$$

The following equation for the electromechanical coupling ratio is found by solving:

$$\eta = 2\pi I_m e_{31,f} z \tag{2.10}$$

The circular plate formula is utilized [67] to get the natural frequency:

$$f_n = (\lambda_{01}/r)^2 \sqrt{D/\mu_{eff}} \tag{2.11}$$

where λ_{01} corresponds to the (01) vibration mode eigenvalue. The total mass of the composite disk, m_d and the shape function is used to determine the modal mass:

$$m_d = (\rho_{\rho\rho} t_{\rho\rho} + \rho_{be} t_{be} + \rho_{a\rho} t_{a\rho}) \pi r^2 + \rho_{te} t_{te} \pi {r_{te}}^2 \tag{2.12}$$

$$m_m = m_d * 2 \int_0^1 \varphi(x_\theta)^2 x_\theta dx_\theta \tag{2.13}$$

where the densities of the distinct layers are $\rho_{\rho\rho}$, ρ_{be}, $\rho_{a\rho}$ and ρ_{te}. Figure (2.1) presents an illustration of the device's functionality.

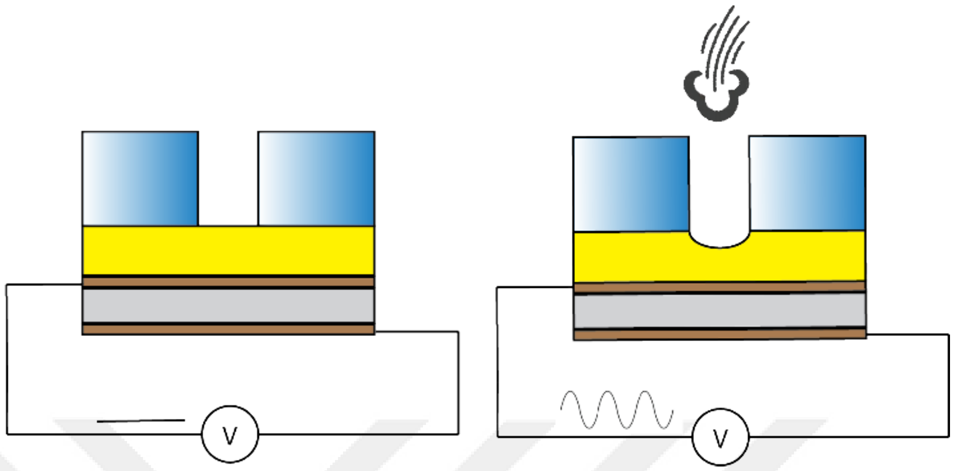

Figure 2.1: Wind energy deforms the plates to create AC output.

2.2 Finite Element Modeling

A finite element model was developed to measure the resonance frequency of the device. An axisymmetric geometry was run under FEM simulation. Figure (2.2a-b.) shows COMSOL® FEM simulation results of the circular plate. The same FEM procedure was adopted in [70] with different geometrical shapes using materials PVDF, ZnO, and PZT.

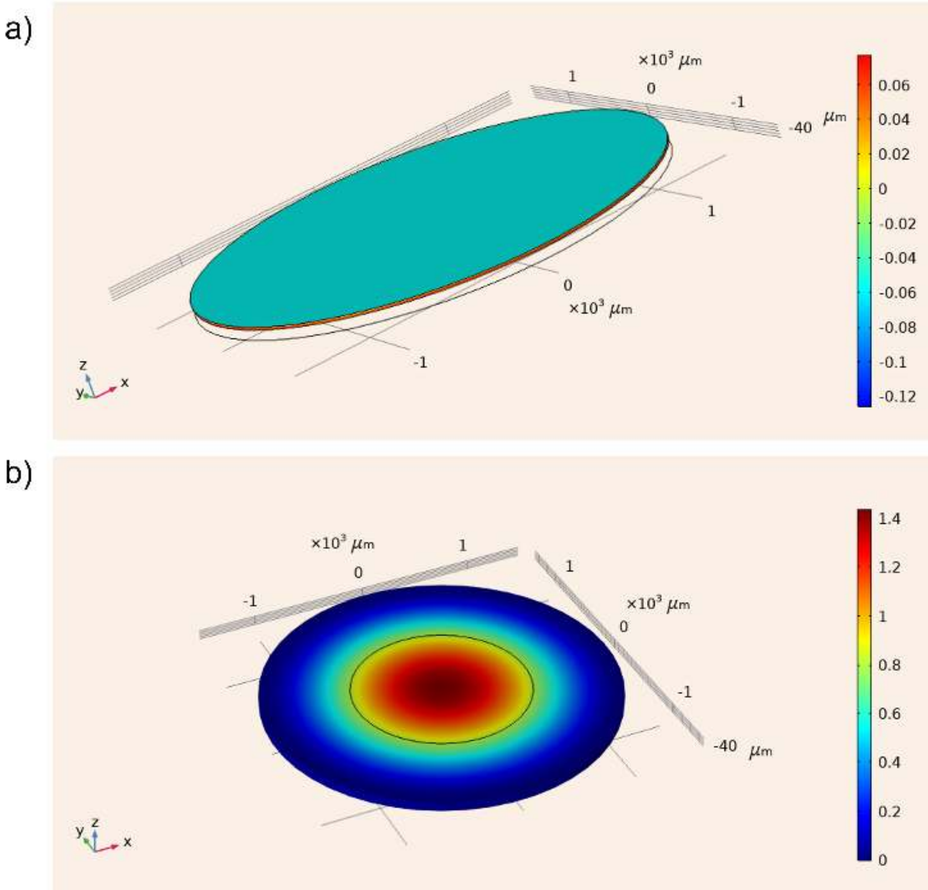

Figure 2.2: a) 400 [N/m^2] pressure applied on the plate where V_{pp} ∼0.2 V flow measured for a singular plate b) A maximum of ∼1.44 µm deflection measured on the surface under 400 [N/m^2] pressure.

Von Mises stress analysis is given in Figure (2.3a-d.).

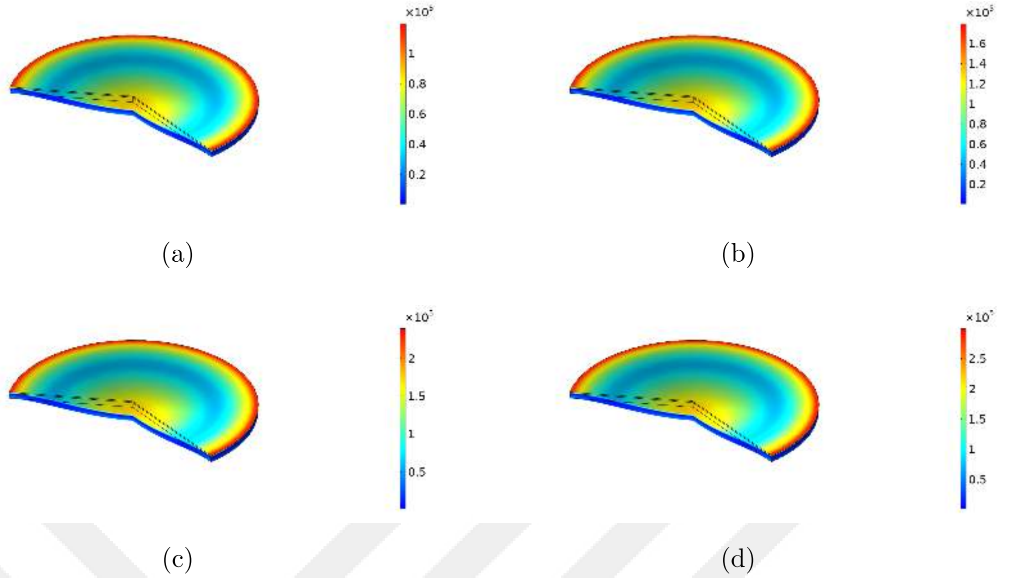

(a) (b) (c) (d)

Figure 2.3: Von Mises stress analysis of the circular plate for different wind pressure inputs: a) 200 Pa b) 300 Pa c) 400 Pa d) 500 Pa pressure.

To visualize the modal frequencies of the circular plate, a FEM model for modal analysis is given in Figure (2.4a-d.).

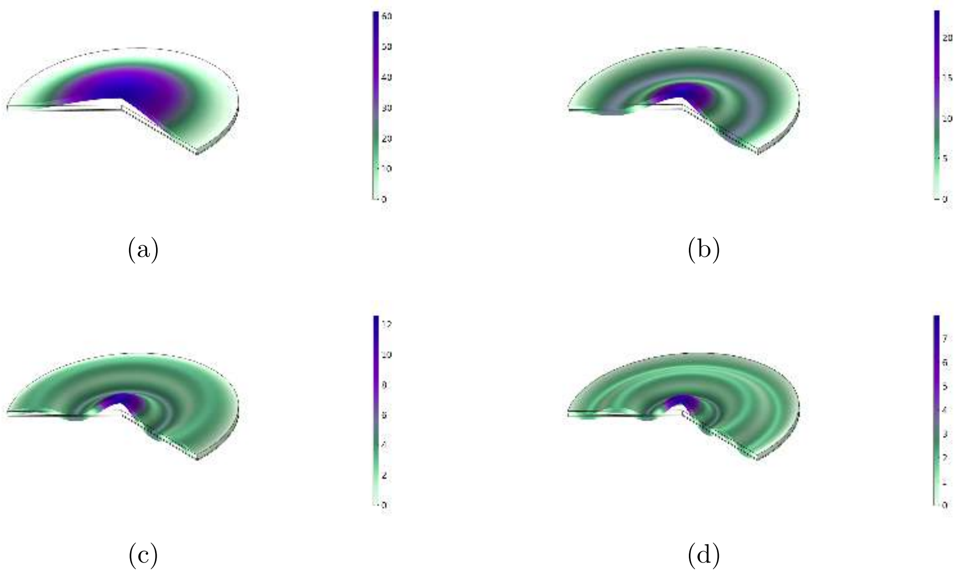

(a) (b) (c) (d)

Figure 2.4: Modal analysis of the circular plate for 4 respective resonance frequencies: a) First resonance frequency: 9.74 kHz b) Second resonance frequency: 36.44 kHz c) Third resonance frequency: 77.30 kHz d) Fourth resonance frequency: 128.91 kHz.

The voltage output plot of the circular plate is given in Figure (2.5). The simulation was run for increasing radius values for 400 Pa pressure input. The voltage values are reported in Volts. The voltage output plot of the circular plate is given in Figure (2.6a-d.). The simulation was run for increasing radius values for 400 Pa pressure input.

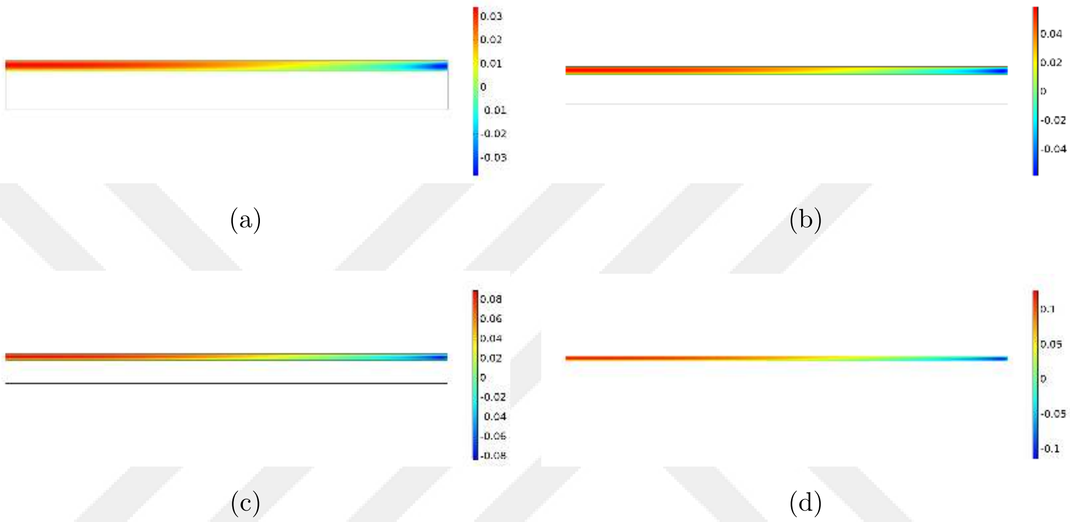

Figure 2.5: The voltage output of the circular plate for increasing radius under 400 Pa pressure input: a) 0.75 mm b) 1 mm c) 1.25 mm d) 1.5 mm radius.

For increasing pressure inputs, voltage outputs of circular plates with varying radius is given in Figure (2.6).

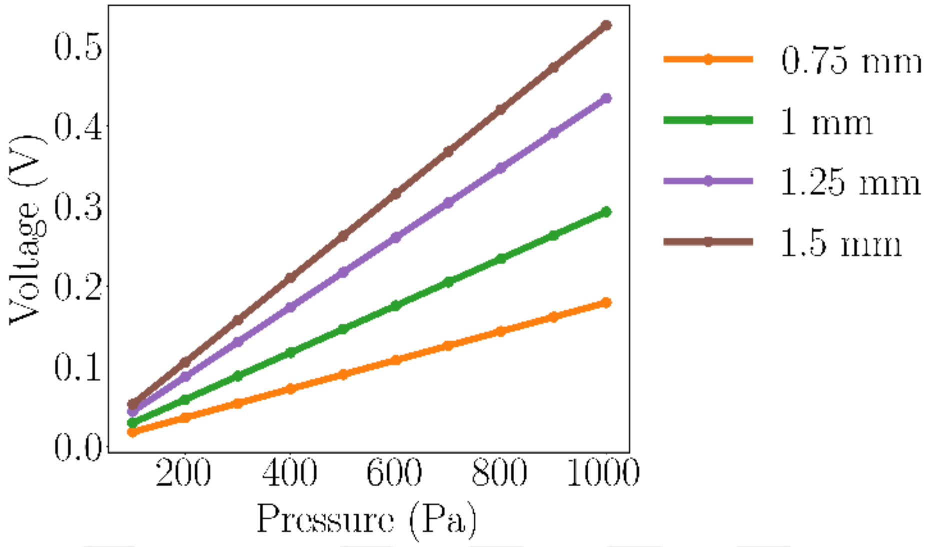

Figure 2.6: Voltage outputs of the circular plates for increasing pressure values.

Displacement of selected points on the plate surface is given together with resonance frequency sweep for increasing radius values in Figure (2.7a-b.).

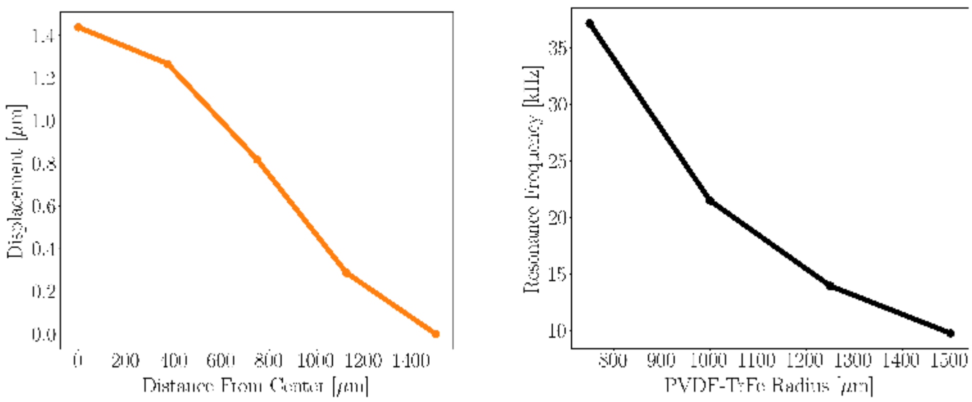

(a) (b)

Figure 2.7: Mechanical properties of the device for optimization: a) Displacement of a selected point on the plate surface for increasing distance from the center b) Resonance frequencies for increasing radius

For increasing thickness values, changing resonance frequency is given in Figure (2.8).

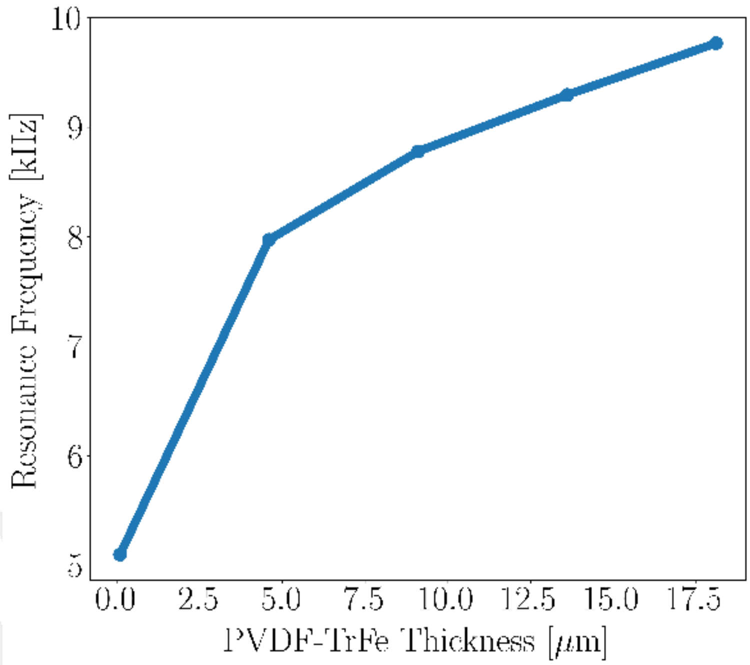

Figure 2.8: Resonance frequencies for increasing thickness.

The frequency response of the circular plate is given in Figure (2.9a-b.). Phase change, amplitude, damping ratio, and quality factor values are given.

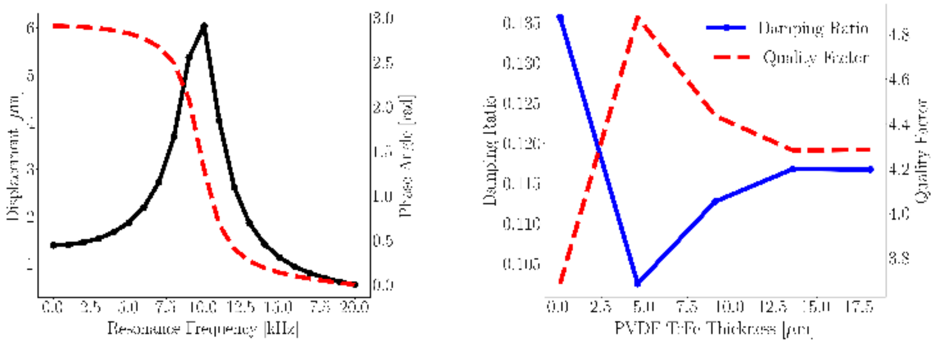

(a) (b)

Figure 2.9: Frequency response plots of the circular plate: a) Frequency response of the plate for phase change and amplitude b) Damping ratio and quality factor of the plate change for increasing piezoelectric layer thickness

The damping factor for increasing plate radius is given in Figure (2.10).

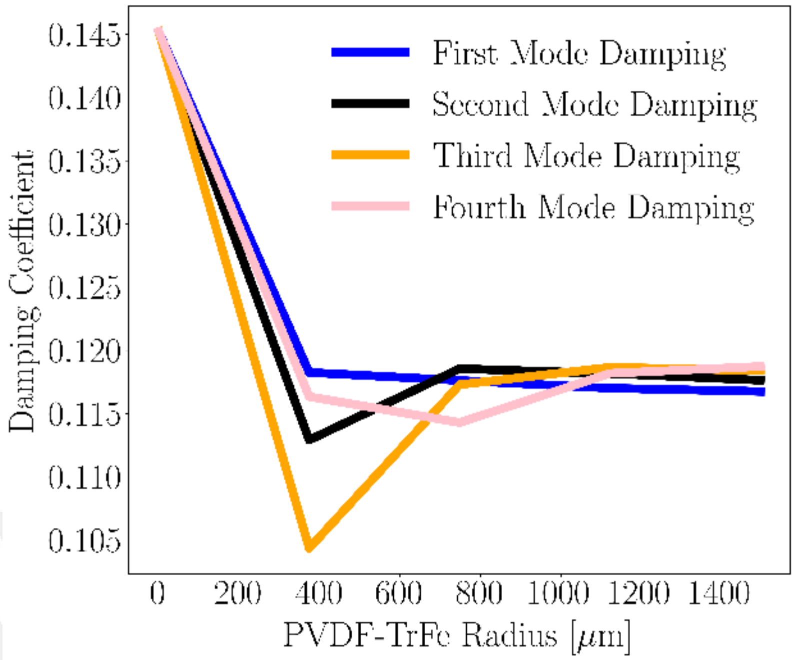

Figure 2.10: Damping factor changes for increasing plate radius.

Quality factor values are given in Figure (2.11) for increasing plate radius.

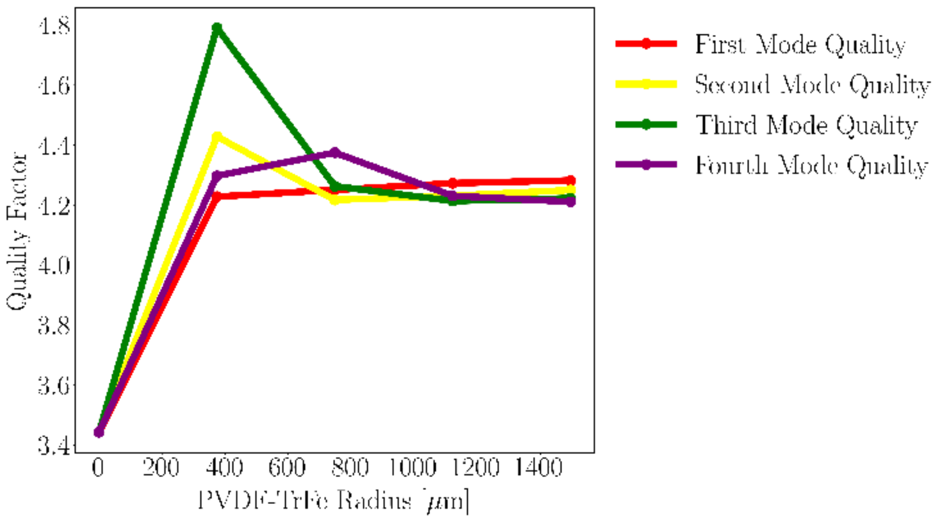

Figure 2.11: Quality factor changes for increasing plate radius.

Chapter 3

STUDIES ON THE PIEZOELECTRIC MATERIAL & FABRICATION

3.1 Literature Search

3.1.1 Introduction

There are various piezoelectric materials used in microsensor design. Ceramics, known as polycrystalline lead zirconate titanate, play a significant role in the field of microtechnology [71]. This is especially true in the areas of sensors and actuators. After attaching to wafer-scale components, piezoelectric PZT material serves as a ground to ultra-precision levels to achieve in-situ thinning that results in thicknesses much below 50 millimeters [72]. Surface roughness and particularly homogeneity of the ceramic component are crucial to the device's operation.

The recent research effort in this field has led to considerable advancements in method, and the technique can now be feasible for flexible bulk assembly and integration. Concerns regarding using complex substances in industrial settings, such as lead, are driving the primary focus of research efforts. Relaxor ferroelectric materials can be identified by a diffuse dielectric phase transition event. This phenomenon indicates that the dielectric permittivity of these materials varies with both frequency and temperature. The adoption of these materials for actuators is still in the very early stages, even though they have demonstrated clear superiority for particular electro-acoustic applications. In general, the qualities of films are not overly sensitive to the production method utilized to make the films [71].

Sintering aid and processing temperature are the two most essential elements that determine the characteristics of the material. Compared to the relative permittivity of equivalent bulk ceramics, the bulk can be approached by specific thick film compositions in relative permittivity. However, due to clamping and the development of secondary phases, piezoelectric and ferroelectric capabilities often decrease to between a quarter and a third of their original value [71].

Statistics on the functionality of experimental devices based on GaN were given by Shur et al. Because of the impact that it has on the operation of field-effect transistors and light-emitting diodes, the piezoelectric effect in III–V nitrides like GaN has been the focus of a great deal of research and investigation [73]. Because of its broadband gap is a potential contender for use in high-power, high-temperature, or radiation-resistant electronic applications, especially over 180 degrees Celsius [71].

3.1.2 Different Types of Piezoelectric Materials

GaN can cancel out any piezoelectric charge produced due to a strain applied to the material. Strittmatter employed Schottky diodes on n-GaN to impede the screening effect so that they could reduce the impact size [74]. AlN, an additional group III–V nitride with a wide band gap of 6 eV, has also been thought about for use in surface wave technology in the form of a thin film. Low deposition temperatures allow for compatibility with traditional integrated circuit technologies [75, 76], and the broadband gap gives high resistivity, which helps to decrease dielectric losses [77].

Since the polar surface is dominant in the growth mechanism of ZnO, a wide variety of piezoelectric nanostructures can be created. It has also been employed in the more common thin film form, sputtered onto a 1.5 mm silicon nitride membrane to create acoustic devices such as small microphones or loudspeakers for cellular phones or earphones [78]. Cantilever actuators constructed from ZnO have been produced and characterized for use with this material.

Article [79] provides a comprehensive analysis of lead zirconate titanate (PZT) based piezoelectric materials, including but not limited to bismuth sodium titanate, alkali niobates ($ANbO_3$), and non-perovskite ferroelectrics. Humans absorb 30 to 70% of breathed lead via their respiratory tracts. With a provision for monitoring every six months, the acceptable range for lead in the blood is between 1.45

and 2.4 mol/L [80, 81], depending on how well the occupational exposure is regulated. Lead-free piezoelectrics include perovskite-type (ABO_3) ferroelectrics. These materials include $BaTiO_3$ (BT), $(Bi_{0.5}Na_{0.5})TiO_3$ (BNT), $KNbO_3$, $NaTaO_3$ and others [79]. The most significant limitations are typically low Curie temperatures (T_c), difficulty in poling treatments, or poor relative densities [80]. However, these issues can be resolved by adding dopants, which improve the piezo characteristics of the material. According to what was found by researchers and presented in [79], the value of d_{33} The pure BNT system can be found between 57 and 64 pC/N. According to Li et al., desired piezoelectric qualities can be produced by combining BNT, BKT, and BT to form a ternary system known as BNT–BKT–BT [81]. They concluded that the dielectric constant and d_{33} go up as the value of x goes up, peak at a value of 150 pC/N when x is equal to 0.035, and then go down again after that. According to these characteristics, the compositions close to the MPB exhibit comparatively high piezoelectric and ferroelectric activity. Under extreme heat conditions, tungsten-bronze piezoelectric ceramics may be employed as sensors, single crystals for electro-optics, and other applications. Doping $Sr_{(2-x)}Ca_{(x-)}NaNb_5O_{15}withLa_2O_3$ was investigated by Matsuo and colleagues, who concluded that the material obtained a dielectric constant of 1662, a Curie temperature of 298 degrees Celsius, and a spontaneous polarization of 10.7 µC/cm^2. According to this study, it appears that lead-free SCNN has the potential to be utilized in electromechanical applications [82, 83, 84, 85]. Both semi-crystalline polymers and piezoelectric composite polymers, which are both forms of bulk polymers, function according to distinct theoretical foundations [86]. "Poling" polymers refers to the process of realigning the crystallites inside the polymer bulk media, and it is performed by providing a strong electric field to the material while it is subjected to a high temperature. This procedure is carried out in order to realign the crystallites. In order to apply the high voltage throughout the polymer, conducting electrodes must be deposited on both surfaces of the polymer sheet. The voltage that is being applied could be a direct current, an alternating current with a sinusoidal waveform, or a triangle low-frequency waveform [87]. The roughness of the polymer film surface can be compensated for by using corona poling, which does not need electrode deposition on one side of the film [88]. If the poling procedure is done a few degrees above the polymer's glass transition temperature, the dipoles may be aligned using an external electric field [88].

Because the polymer has a low impedance, piezo composites are the preferred material for acoustic devices [89]. A wide variety of permutations is possible for the arrangement of ceramic and polymer composites [89]. Various numerical and analytical models have been devised to estimate the chemical properties of composites of this kind [90, 91, 92].

Voided charged polymers are similar to piezoelectric materials in their behavior because they contain dipoles inserted inside voids. Whenever a field is applied across the voids, charges of the opposite sign are pushed and implanted on each side [93]. The direction in which the electric field is delivered determines which charge is accelerated and implanted first. VCPs have a more complicated structure than other capacitor types since they hold varying charges in suspension using a variety of springs and dampers [94]. Because a structure of this complexity possesses a resonant mechanical response, the overall displacement of the structure is subject to change depending on the frequency being applied [88].

3.1.3 The PVDF-TrFe Piezoelectric Polymer

The polymer PVDF can be stretched in both the longitudinal and the transverse directions, which allows it to be used to form a bi-oriented film [95]. If PVDF proves to be an excellent candidate for the fabrication of piezo films, the P(VDF-TrFE) copolymer may also be poled [95]. This particular copolymer will crystallize immediately in beta form as a result of the replacement of a few of the VF2(CH2-CF2) molecules in the PVDF with VF3 (CH-CF3) molecules [95].

In the study of Mohammadi et al., Fourier transforms infrared spectroscopy was used to evaluate the influence of biaxial orientation and deformation rate on the microstructure of stretched PVDF samples, and wide-angle X-ray diffraction was used to confirm the findings of the FTIR analysis [96]. FTIR spectroscopy is a well-established method for determining whether or not there has been a shift in the amount of b-phase present in PVDF films. It has been demonstrated that an additional transition of the non-polar a phase into the polar b crystallites occurs when the stretching rate is 10–50 cm/min [96]. Polarized PVDF films have fairly balanced piezoelectric activity in the film plane, unlike uniaxially oriented PVDF films, which have more significant piezoelectric coefficients [97]. This is because polarized PVDF films are oriented in two orthogonal directions. The crystalline structure of PVDF is directly responsible for the material's electrical characteristics [98, 99, 100, 101, 102].

Today, various different polar crystals have been described for PVDF. These modifications are designated as b (form I), g (form III), d (form IV), and e (form V) [103]. Only when the stretch ratio is more than five is the melt-crystallized PVDF capable of being transformed into the b-phase [104]. In order to produce polar b-phase PVDF straightforwardly, one must either cast PVDF from solutions of hexamethyl phosphoric triamide or quench molten PVDF under high pressure. Both of these processes are required. Both of these methods produce the same result [104]. The electrical charge in the matching PVDF film is significantly lower than that in the 55 mol percent VDF copolymer, which has the biggest dielectric constant and the most considerable electric current [96].

An uncommon negative longitudinal piezoelectric effect was seen by Katsouras et al. in the ferroelectric polymer poly(vinylidene fluoride) (PVDF), as well as its copolymers with trifluoroethylene (P(VDF-TrFE)) [105]. It seems inconceivable that the polarization-biased electrostrictive contribution of the crystalline component is the only factor responsible for this event [105]. Electromechanical contact between crystalline lamellae and amorphous areas is the cause [105]. The so-called dimensional model, a commonly accepted explanation for the negative piezoelectric effect of PVDF, assumes that the dipoles are stiff and maintain their fixed moment and orientation even when the material is mechanically deformed [105].

According to Katsouras et al., applying a positive stress perpendicular to the chains mainly increases the distance between the chains. This is because the interactions between the chains, both van der Waals and electrostatic, are relatively weak. This dipole-induced piezoelectricity process has been verified using quantum mechanical simulations for single-crystalline polymers [106, 107]. P(VDF-TrFE) crystallizes into needle shaped domains, whereas PVDF films consist of massive lamellae, which spread outward from the center. In P(VDF-TrFE) copolymers, an electric field causes electrostriction, commonly known as dipole-induced piezoelectricity. The lattice constant goes down, and in addition to that, the amorphous components that are sandwiched in between the polar lamellas get smaller [105].

PVDF-TrFE was selected as the actuation material for the piezoelectric harvester. Table (3.1) shows the superiority of PVDF-TrFE compared with other widely used piezoelectric materials in terms of voltage output KPI.

Table 3.1: PVDF has a higher g_{33} coefficient than other widely used piezoelectric materials.

Parameter	$BaTiO_3$	Quartz	PZT4	PZT5H	PVDF-TrFe
d_{33} $[10^{-12}]$	180 [108]	2.3 [109]	289 [110]	593 [111]	-38 [110]
$\rho [kg/m^3]$	6010 [112]	2620 [113]	7500 [114]	7500 [115]	1800 [116]
ϵ_x/ϵ_0	1557 [108]	5 [109]	1300 [109]	3400 [109]	9.4 [116]
g_{33} $[10^{-3}]$	13.06	51.98	25.12	19.71	456.79

3.2 Characterization of PVDF-TrFe Thin Films

PVDF-TrFE has a dual-phase microstructure consisting of and phases where the percentage of the beta phase determines the stiffness and crystallinity of the film. Figure (3.1a-b.) represents the test setup used for stress-strain curve plotting, and Figure (3.2) represents the stress-strain curve in the elastic region for the semi-crystalline PVDF-TrFE copolymer.

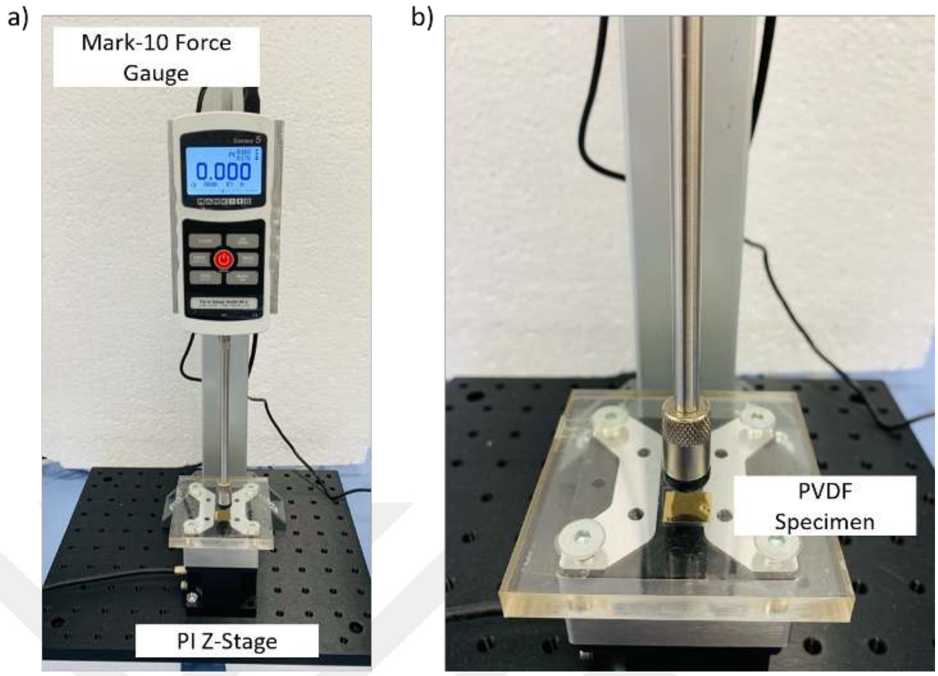

Figure 3.1: a) Compressive tests were done using a force gauge and PI L-306 Compact Precision Z-Stage b) Metal coated PVDF specimen was used for the experiment.

According to the curve, the polymer has a Young Modulus of 0.87 GPa, proving its robustness. In addition to the high stiffness of the polymer, the flexibility of the film is shown, which indicates that PVDF-TrFE is a suitable candidate for energy harvesting applications where flexibility and mechanical robustness are required [117].

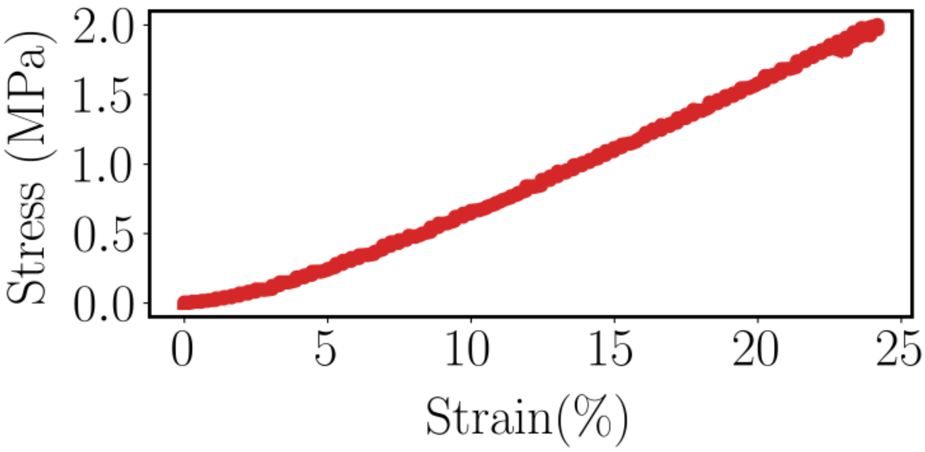

Figure 3.2: Stress-strain plot of the material resembles a linear curve in strain levels as high as 25%.

According to equation (1), where g_{33} is piezoelectric voltage coefficient, d is thickness, and s is applied stress, the voltage output of a piezoelectric film is directly proportional to the applied stress on the film. Figure (3.3a-b.) demonstrates the flexibility of the film under a microscope.

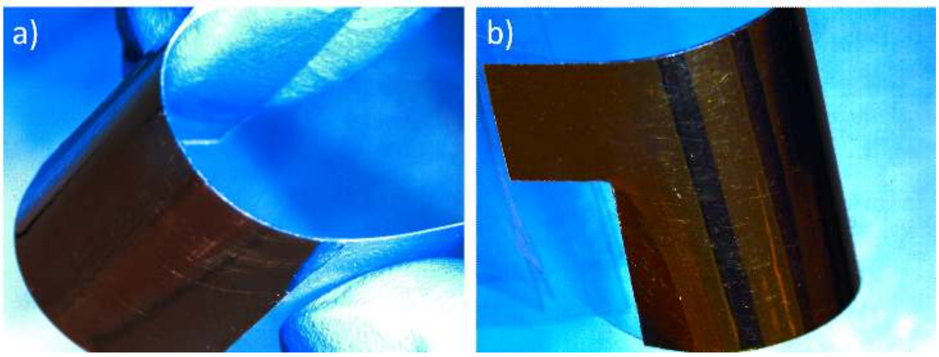

Figure 3.3: a) Optical image representing the flexibility of the harvester b) PET layer was used as a substrate for the piezoelectric layer to bend without going into a tear, permanent deformation.

Also, based on the stress correlation with the strain, which is realized by Young's Modulus (equation 2), the higher magnitude for E results in higher voltage output, which is crucial for energy harvesters.

$$V = g_{33} ds \tag{3.1}$$

$$V = g_{33} dE\varepsilon \tag{3.2}$$

In this way, tunability of phase percentage by chemical methods or electrical poling of the film results in higher crystallinity, which determines the young modulus of PVDF-TrFE films. Thus, we utilized FC20 polymer powders with 20 percent mol content of TrFE (phase) to achieve proper flexibility and stiffness. This way, various PVDF-TrFE films with elastic modulus between 0.7-3 GPa can be selected based on the trade-off between the required flexibility and voltage output in a specific energy harvesting application.

PVDF-TrFe material characterizations were determined in terms of thickness, pyroelectric, and ferroelectric measurements. In order to characterize the material, it is necessary to first use 2w% PVDF-TrFE in acetone as solvent (Piezotech FC25). The specimen is then placed on a magnetic stirrer for 1 hour at 80C. The solution was then filtered to make it more homogenous. The filtered solution was spin-coated on glass substrates sweeping between 750 RPM to 5000 RPM. In Sharma et al. [118], spin-coated PVDF on Al substrate was also used to build a pressure sensor for catheter applications. In [119], a thin film was fabricated using a spin coating approach to be used as an active layer for converting mechanical energy to electrical energy. A spin coating routine for a 5000 RPM specimen is given in Figure (3.4).

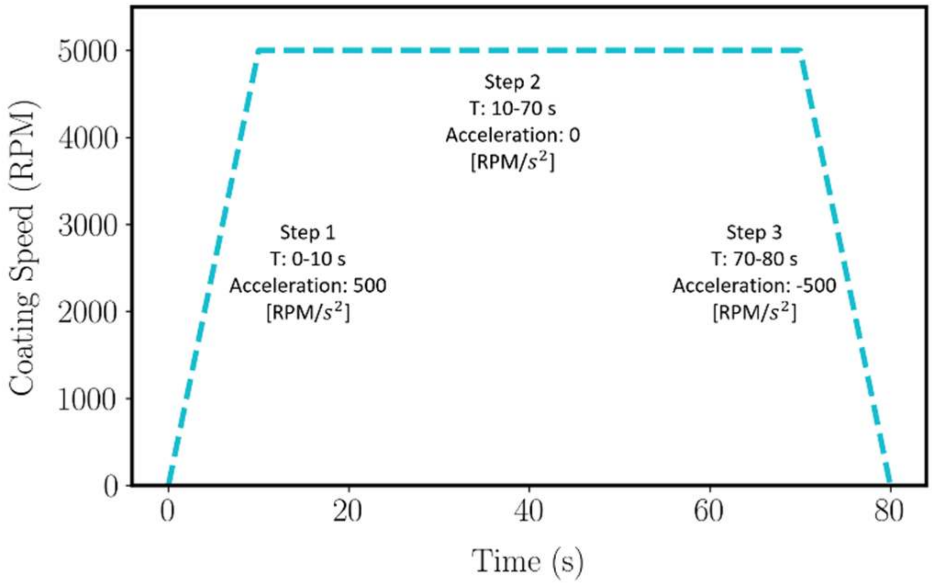

Figure 3.4: Acceleration values were the same in all of the spin-coated samples with different maximum RPM values.

After this operation, the solution was annealed for 1 hour at 140 °C. Figure (3.5) shows the thickness of the deposited layer for different RPMs. Also, Figure (3.6a-d.)) shows the microscope images of the PVDF-TrFe specimen. Table (3.2) shows specimen features that were used in the measurements.

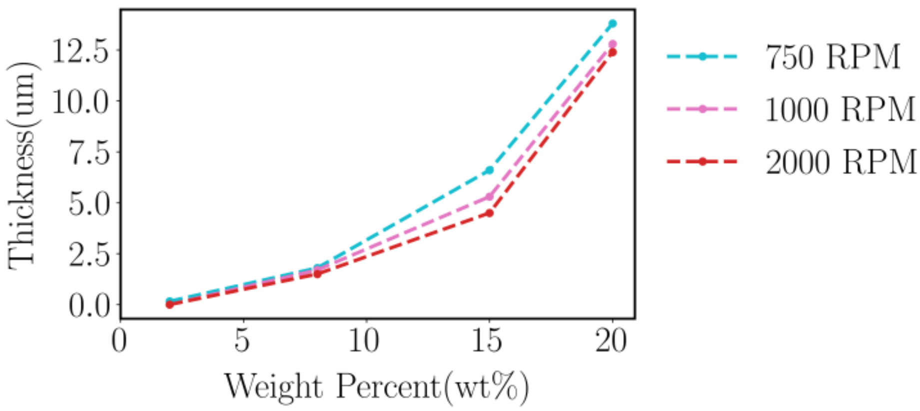

Figure 3.5: Profilometer thickness measurements were taken with Dektak XT for different spin-coated specimens.

In [118], researchers claim that the thickness dropped when the spin speed was increased. Indicative of the stronger piezoelectricity of thinner film, researchers found that the signal output from the PVDF device with a thickness of 1 µm was roughly 1.7 times higher than the signal output from devices with a thickness of 6 µm. This was feasible because higher surface tension is required to produce a thinner film during spin coating. Consequently, thinner films have a higher crystallinity than thicker films. In [119], the PVDF-TrFE copolymer solution with a concentration of 2 percent and the PVDF-TrFE copolymer solution with a concentration of 15 percent were subsequently spin-coated on the substrate to attain the requisite thicknesses of 220 nm and 6.5 µm, respectively.

Table 3.2: PVDF-TrFE 15W% in acetone/DMF spin-coated with 750 rpm and thickness of $6.6\mu m$.

Sample	Substrate	Electrodes	Characterization
1	PET/ITO	Aluminum tape on top and ITO on the bottom	Poled Capacitance: 46 [pf] Area: 240 mm^2 Thickness: 6.6 µm
2	PET/ITO	Aluminum tape on top and ITO on the bottom	Poled Capacitance: 68 [pf] Area: 187 mm^2 Thickness: 6.6 µm
3	PET/ITO	Aluminum tape on top and ITO on the bottom	Unpoled Thickness: 6.6 µm
4	Glass/ITO	Copper tape on the top and ITO on the bottom	Poled Thickness: 6.6 µm

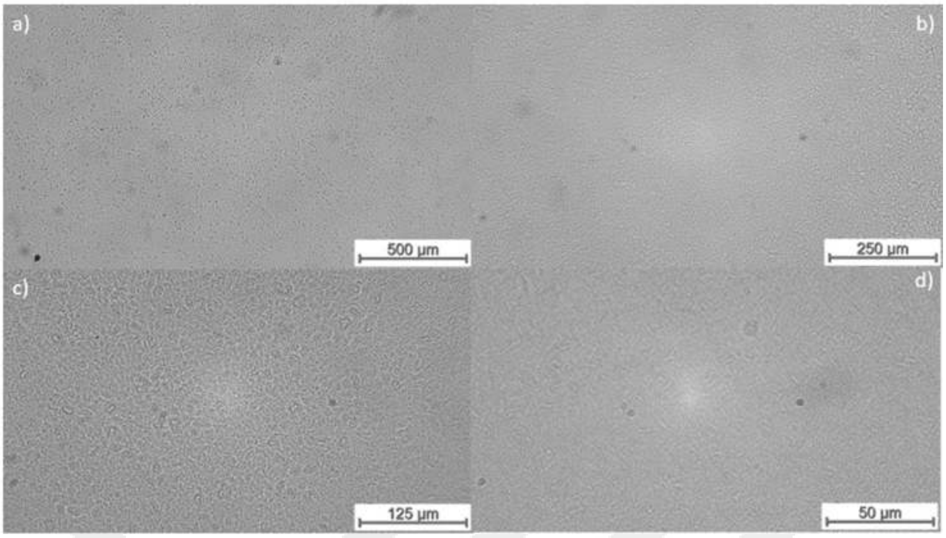

Figure 3.6: Microscopic images of PVDF-TrFe specimen with: 5x (a), 10x (b), 25x (c) and 50x (d) magnification showing desirable surfaces with no defects.

Film formation was not desirable in 5000 RPM spin-coated film as short circuit tests for this specimen failed for most regions when it was spin-coated on ITO glass—indicating non-uniformity or porosity of the surface. Film formation was better in 2000 RPM than in 5000 RPM spin-coated film; however, the short circuit test failed on the edges of ITO glass. A 33wt% PVDF-TrFe (FC25 Arkema Piezotech) solution was too viscous to be squeezed using the pipettes. In conclusion, lower RPMs (2000) resulted in better film uniformity, but acetone seems not to be a suitable solvent for PVDF-TrFE due to its highly volatile nature. Poling was done using the high voltage DC power supply. Poling procedure is given in Figure (3.7), and the poling setup is given in Figure (3.8a-b.). An additional 100 V was applied for 1 µm thickness.

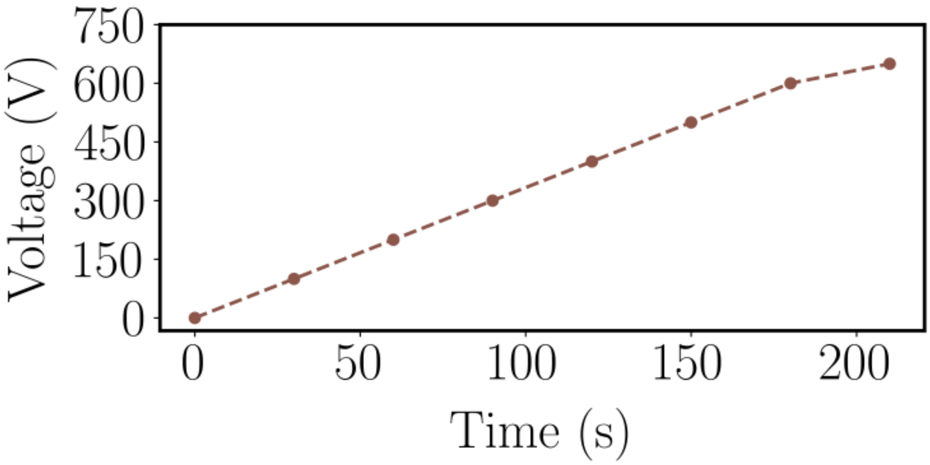

Figure 3.7: The poling process of the 6.5 µm thick PVDF-TrFe material was done in silicone oil to prevent electrical sparks under high voltage.

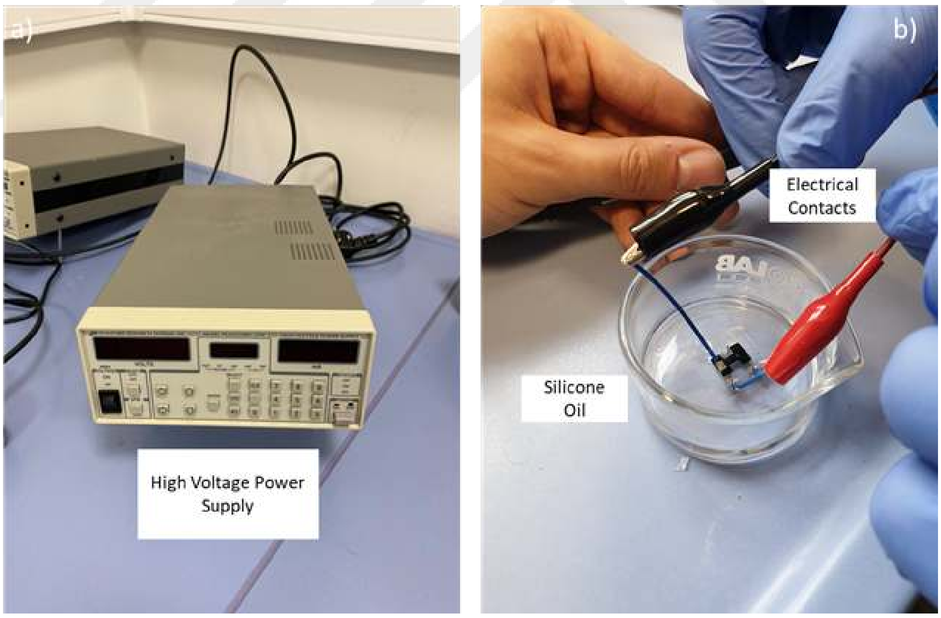

Figure 3.8: a) Voltage values up to 2500 V could be applied with the supply b) The test specimens were immersed in silicone oil to prevent sparks under high voltage.

The approach used in the process for voltage increments utilized a Sawyer-Tower Circuit, which was built for conducting ferroelectric measurements with the specimens. Figure (3.9) shows the result of these ferroelectric measurements, which were conducted with the circuit given in Figure (3.10) using the specimens in Figure (3.11).

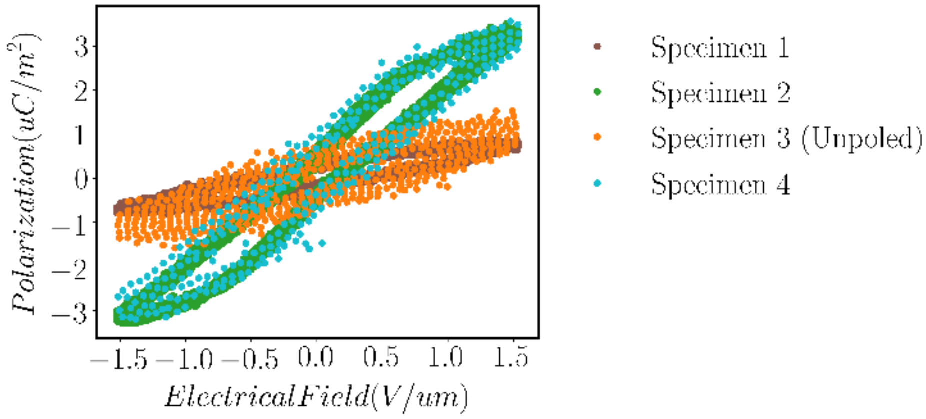

Figure 3.9: Polarization results for 4 different test specimens are given. Measurements are done using triangular waves with 20 V_{pp}.

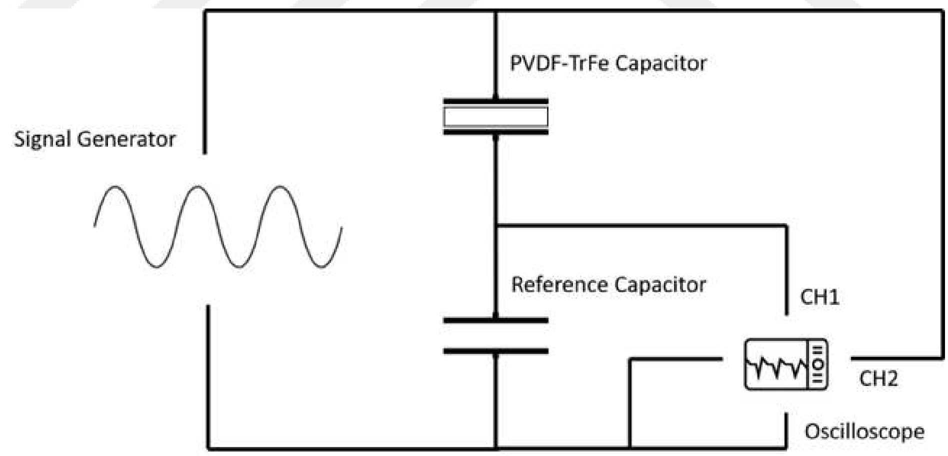

Figure 3.10: Sawyer-Tower circuit built with a reference capacitor having a thousand times higher capacitance than the PVDF-TrFe capacitor.

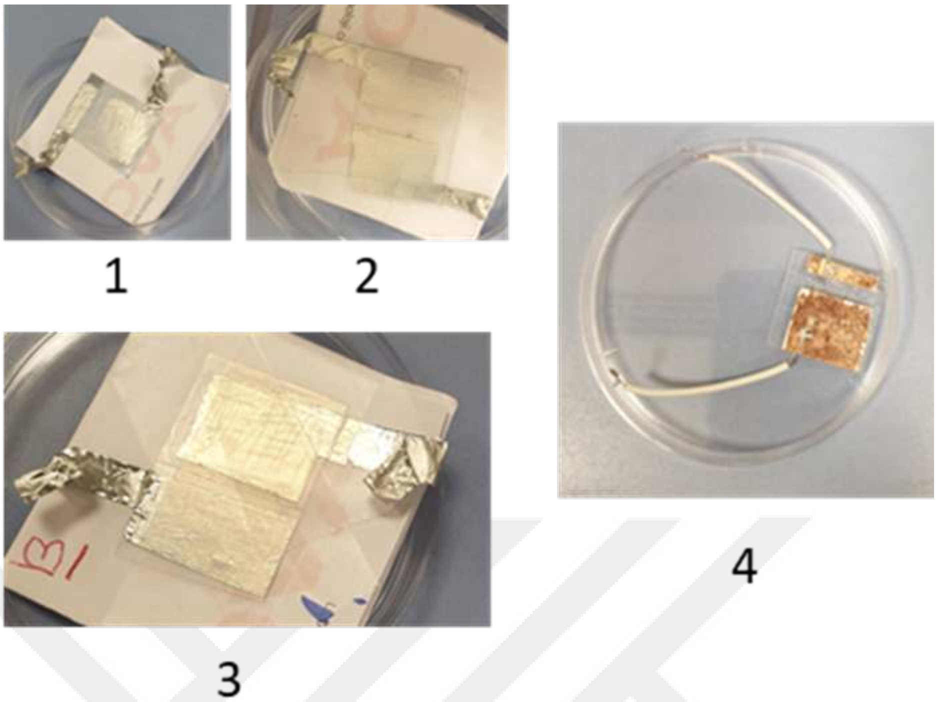

Figure 3.11: Piezoelectric specimen numbers match the test specimen numbers given in Table (3.2).

3.3 Fabrication of Flexible Piezoelectric Energy Harvesters

To validate the fabrication flow, a 3 mm diameter hole on a 10×10 mm PET sheet was created using a mechanical cutter. A thin double-sided tape was put on top of a supportive PET cut into a 7×10 mm rectangle. Another PET sheet, which PVDF will later replace, was then cut according to design constraints. This layer also had parts shaped as the contact pads with 3×3 mm dimensions and was attached to the double-sided tape. In the first step, plain PET sheets were cut in 10×10 mm size with a mechanical cutter to fabricate the device. The sheets were 140 µm thick and cut with a laser to form 3 mm diameter circular cavities. A 65 µm thick double-sided tape was then put on the PET. The tape was used to fix the PolyK PVDF film on the sheet. In addition, the tape was used as the structural layer for the harvester, moving the piezoelectric layers away from the neutral axis. Figure (3.12) shows the fabrication steps used to fabricate the PEH prototypes.

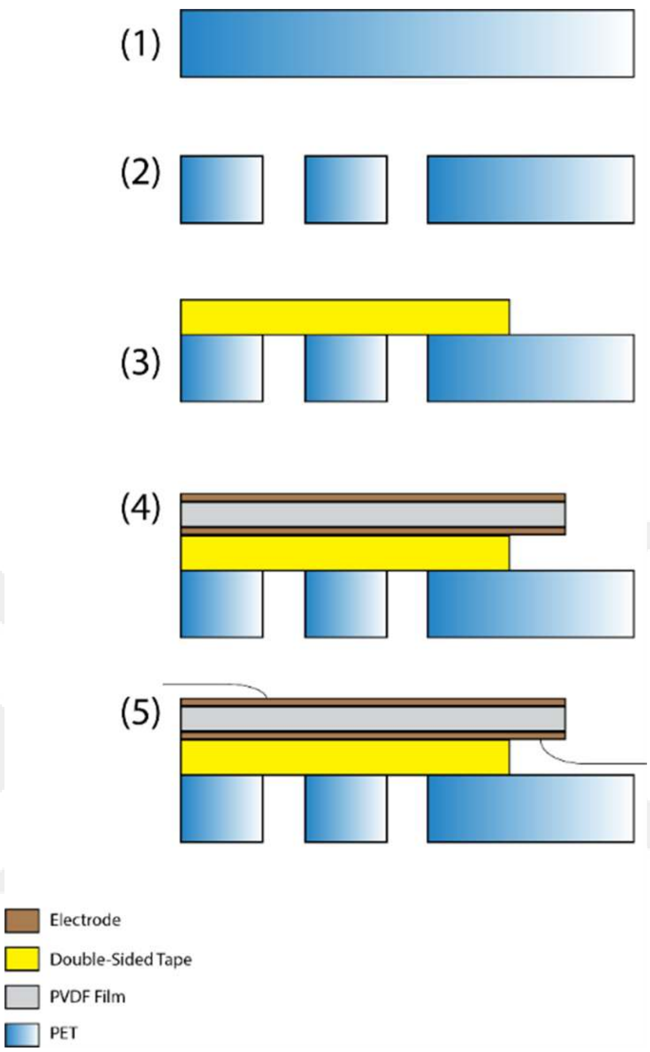

Figure 3.12: (1) Plain PET sheets were cut in 10×10 mm size with a mechanical cutter device (2) Sheets were cut with a laser to form 3 mm diameter circular cavities (3) A thin double-sided tape was put on top of the PET (4) The tape was used to fix the piezoelectric film on the sheet (5) Bonding connections were realized.

An 18 µm PVDF-TrFE layer was then placed on the double-sided tape. Two 3×3 mm electrode pads were cut out of the PVDF film to make bonding easier while getting connections from the device. The sheet was metal coated on both sides. Using the described process, circular plate energy harvesters with 3 mm diameter were fabricated, as shown in Figure (3.13a-b.). Another design is proposed in Figure (3.14a-b.). The acoustic resonator tube length was fixed to 140 µm in all prototypes.

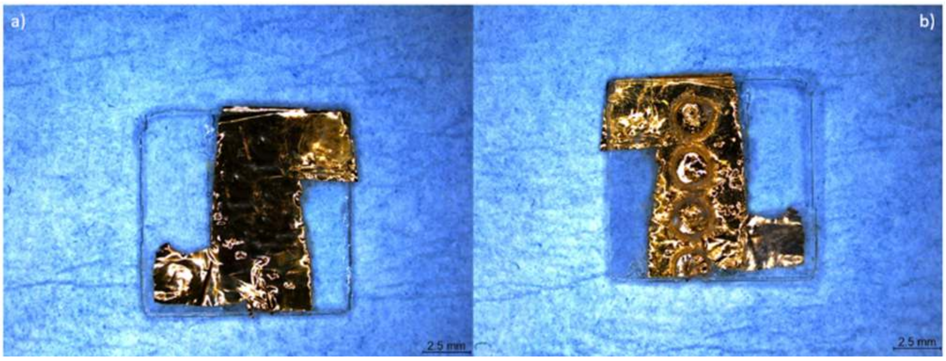

Figure 3.13: Optical image of the fabricated sensor (First Design).

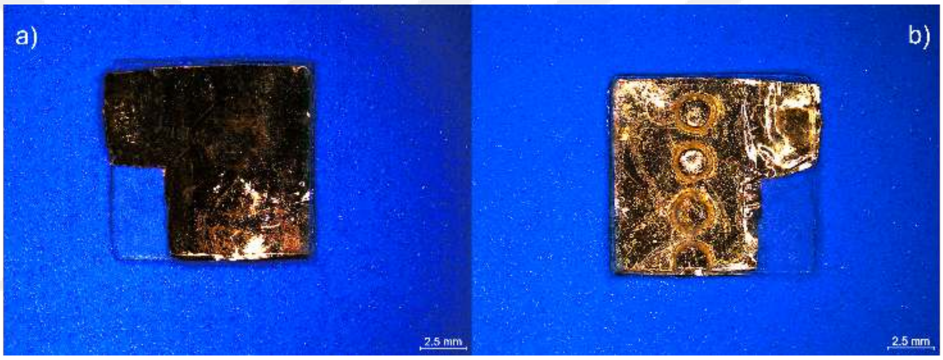

Figure 3.14: Optical image of the second design for harvester.

Chapter 4

TESTING

The experiment platform was built as shown in Figure (4.1a-b.). The setup consisted of a Pulse Width Modulation (PWM) 4-wire fan, an Arduino Uno, a dry air supply, and a BMP280 pressure sensor breakout board from Adafruit. The output properties of the wind setup were studied experimentally and provided in Figure (4.2a-d.).

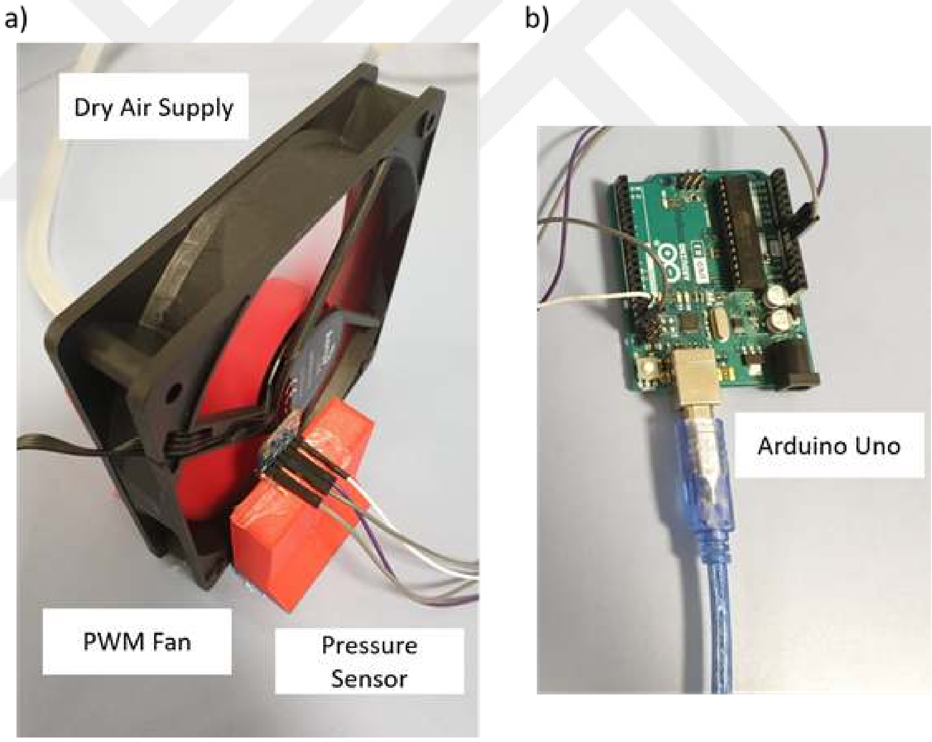

Figure 4.1: a) Test setup was built using 3D printed parts which have a cavity for dry air supply and a surface to fix the pressure sensor b) SPI communication was used to get the values from the pressure sensor.

A code was developed to measure the pressure dynamically from serial pins.

Serial Peripheral Interface (SPI) protocol was used for the communication. A unique test setup was built using 3D-printed parts. Dry air was flown towards the fan's turning propeller, which creates pressure fluctuations by creating intervals. The frequency of these intervals was set by changing the PWM frequency of the fan and operating voltage value. PEH was fixed close to the fan to be vibrated by these fluctuations, creating alternating voltage. The maximum wind speed measured was 20 m/s. The rotational speed of the fan was validated using a tachometer. Figure (4.3) shows the current measurement's experimental circuit and oscilloscope output.

The current output of the harvester was measured using an oscilloscope. The tested harvester and the circuit schematic are given in Figures (4.4) and (4.5a-b.). The output voltage was converted to the current by dividing the peak-to-peak CH2 output of the oscilloscope with the resistance value (1.5k Ω).

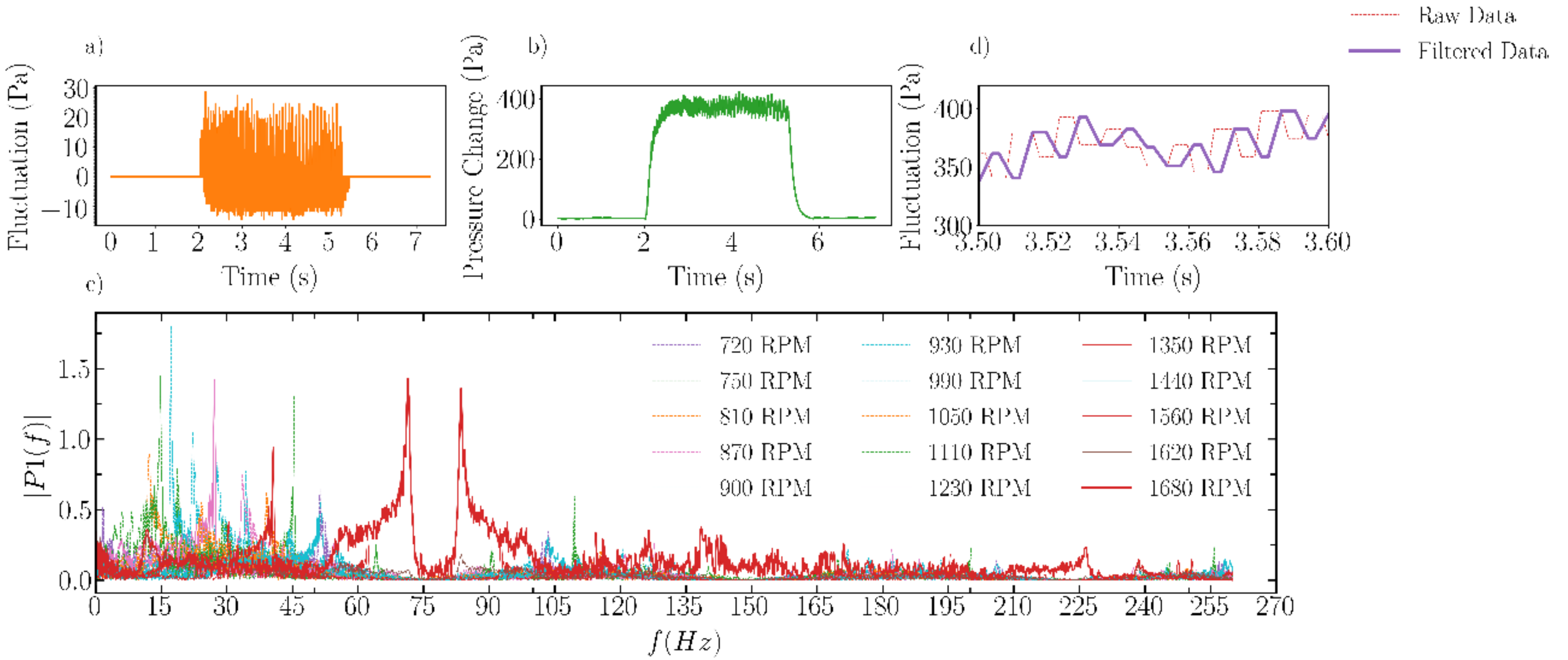

Figure 4.2: a) Pressure fluctuation spikes were plotted for 1680 RPM measurement showing peak-to-peak 45 Pa pressure changes per hit b) Using the dry air supply, 400 Pa of pressure could apply to the piezoelectric plates c) Sweeping through 720 RPM to 1680 RPM tests using the PWM fan, FFT was done to each test data extracting the dominant fluctuation frequencies. 1680 RPM was chosen for the application for having the highest fluctuation frequency having dominant peaks at 72 Hz and 84 Hz d) Testing data was filtered through moving median filter by taking the average of last 5 values. The 0 Hz noise in the FFT plots were eliminated using filtering.

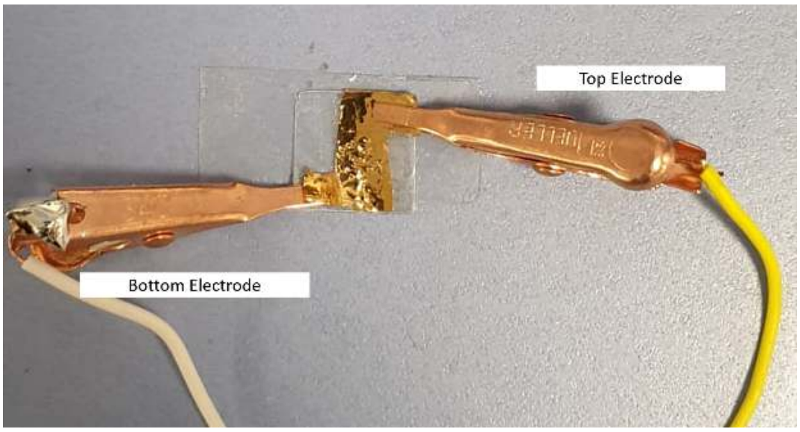

Figure 4.3: The setup was used to measure the current output from the PEH by applying pressure on top of the sensor; the voltage output was later converted to the current; two flat tip crocodile wires were used to get contacts from the bottom and top electrodes.

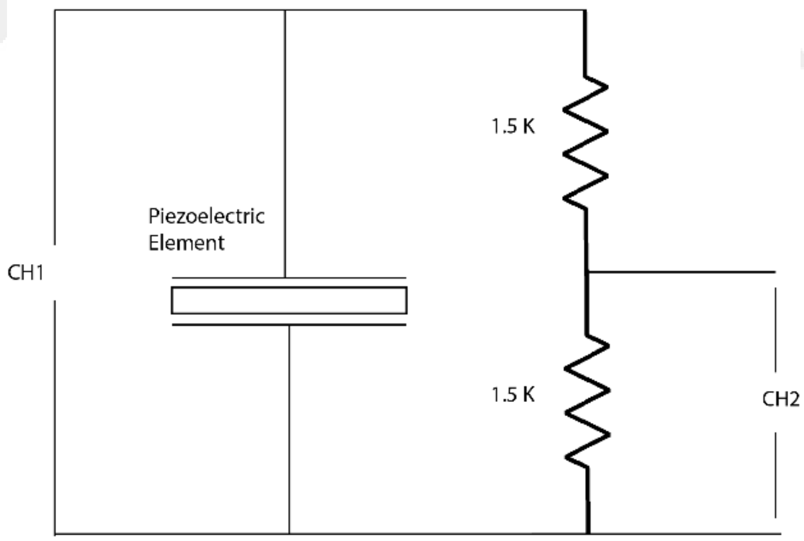

Figure 4.4: Circuit model used for harvester test. A 1.5k Ω resistor was used in the measuring circuit. CH1 and CH2 are the two channels of the oscilloscope showing two different outputs which can be converted to the output current.

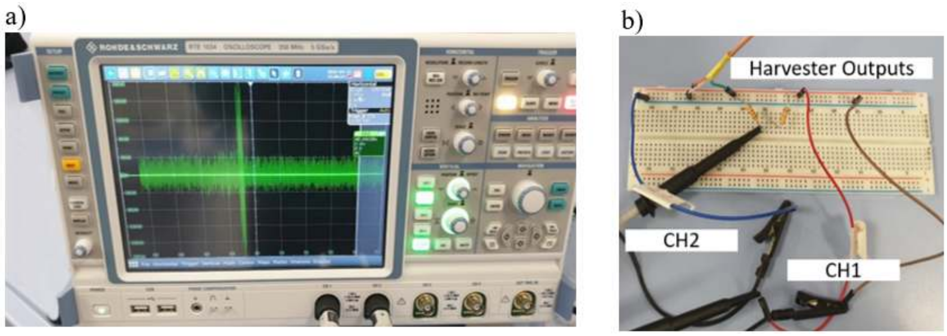

Figure 4.5: a) Oscilloscope output from the current measurements b) 1.5 kΩ loads used in the circuit.

The procedure was applied to both harvester designs.

Chapter 5

RESULTS AND DISCUSSION

The research presents two 10 × 10 mm^2 transducers built on the PET layer. Low resonance frequency PEHs can benefit from this because most environmental vibrations are at low frequencies. Using measured layer thicknesses, the neutral axis and its distance from piezoelectric midplanes were estimated; z = 74 µm. Figure (5.1) and Figure (5.2) represent the voltage and current output of the harvester having the first design, respectively, while Figure (5.3) shows the oscilloscope output for the voltage values.

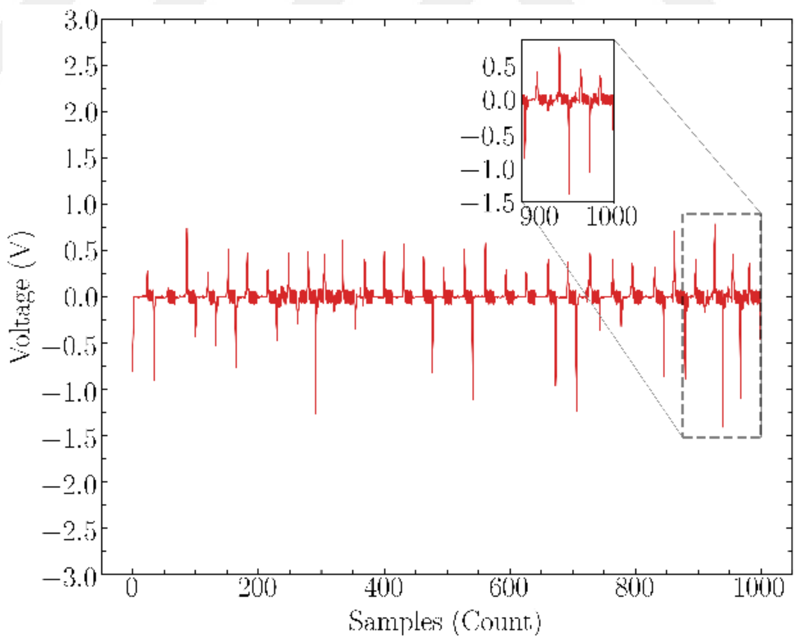

Figure 5.1: The maximum peak-to-peak value seen was 1.4 V under impulse (First Design).

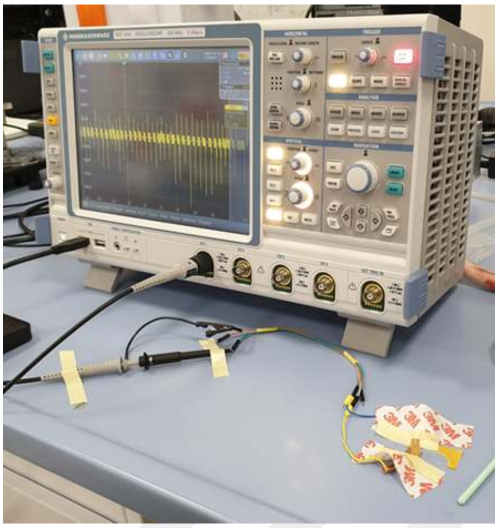

Figure 5.2: Voltage output of the harvester under impulse measured from the oscilloscope.

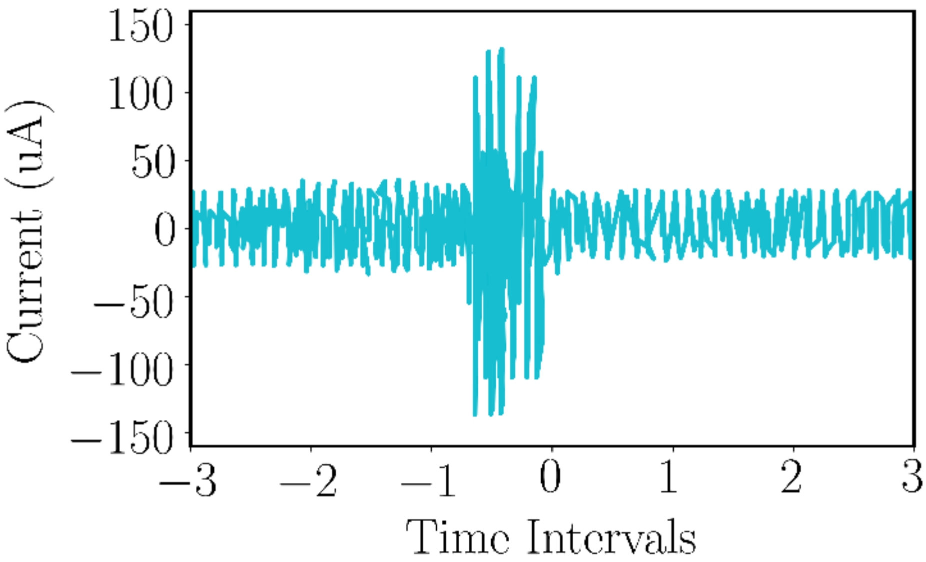

Figure 5.3: The maximum current was 136.9 μA under impulse when taking the average of the peak values (First Design).

It is also worth noting that the piezoelectric material can withstand significant degrees of strain. Having higher power output, the second harvester design was evaluated under a wind test setup. Figure (5.4) demonstrates the harvester's voltage, current, and power output on the same time scale.

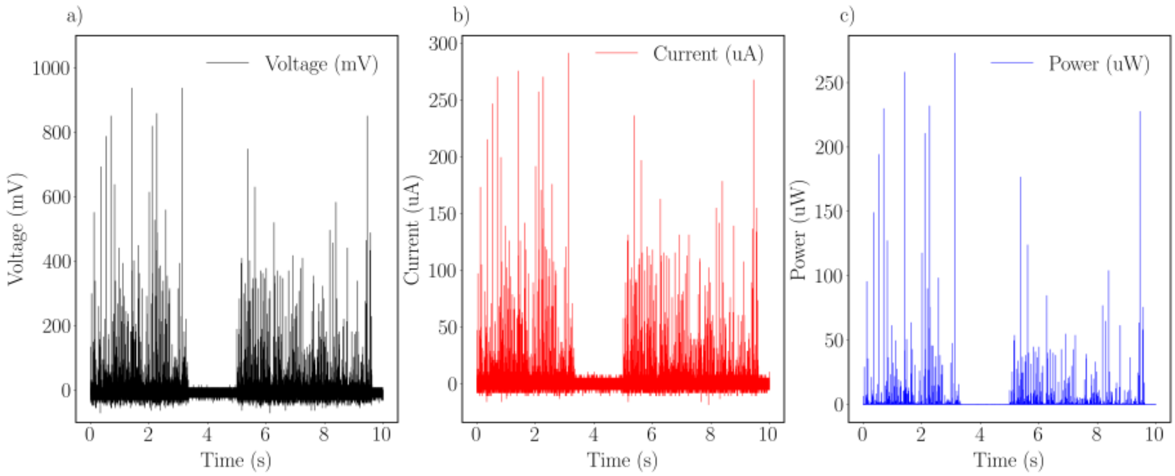

Figure 5.4: a) The maximum voltage obtained from the wind setup was V_{max} = 937.01 mV while the sensor was connected to the current measurement circuit b) The maximum current obtained from the wind setup was I_{max} = 291.34 µA c) The maximum power obtained from the wind setup was P_{max} = 272.99 μW.

Figure (5.5) shows the peak-to-peak voltage graph obtained from the Picoscope for the second design. It is worth noting that the output voltage produced is 6.61 V_{max}.

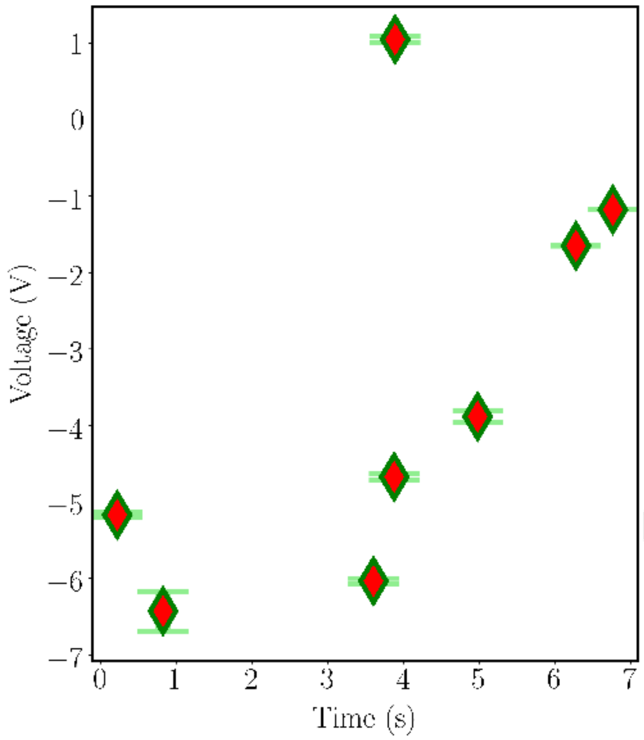

Figure 5.5: The output voltage measured from the sensor. The output voltage produced from the sensor was also validated by a multimeter under impulse (Second Design).

Figure (5.6) shows the current output of the harvester under the impulse to make a comparison with the first design. The power output difference between the two designs is mainly based on the effective piezoelectric layer area, where the second design has a 36.2% larger piezoelectric layer area compared to the first design.

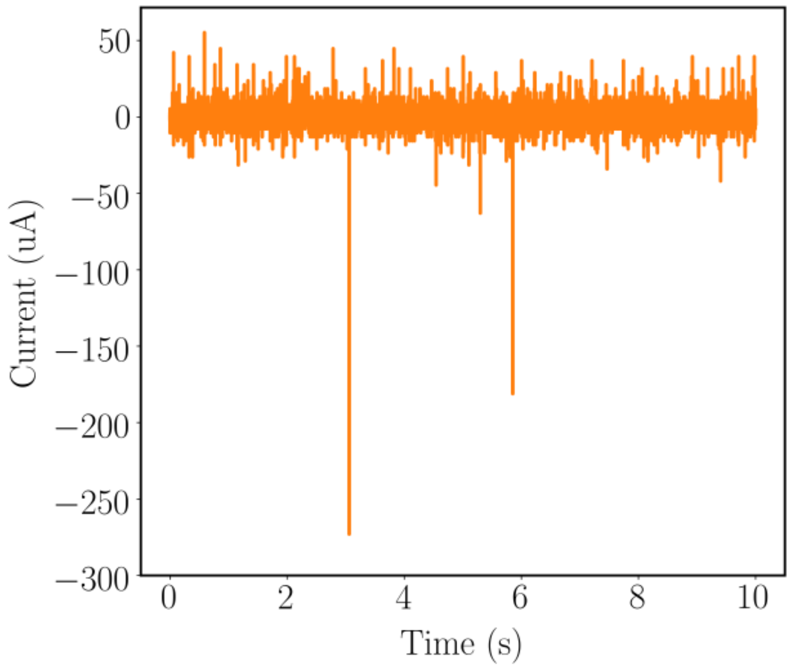

Figure 5.6: The output current from the sensor under impulse current of $I_{max} = 273$ µA (Second Design).

Impact applied to the sensor for measuring a capacitor charge-discharge curve. The circuit given in Figure (5.7) was used for rectifying the AC output and capacitor charging, and the output is shown in Figure (5.8).

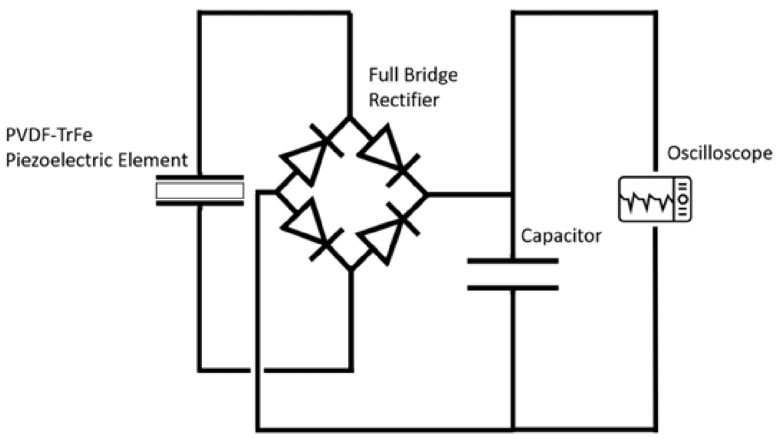

Figure 5.7: 104 nF ceramic capacitor was used for the circuit

After the force was released from the piezoelectric element, the capacitor charge was discharged due to the 1 MΩ oscilloscope input impedance.

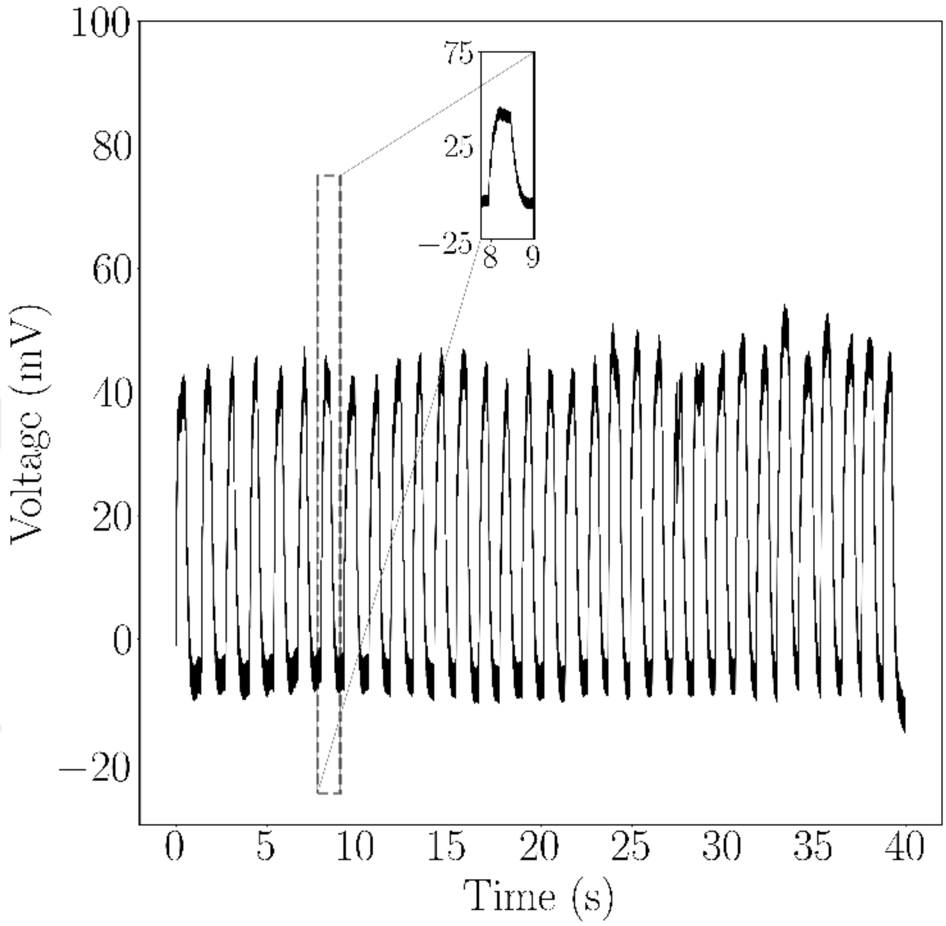

Figure 5.8: A single impulse contributes to a V_{max} ~64.4 mV

This experiment runs for 10k seconds to show the stability of the capacitor charge. The test results are given in Figure (5.9).

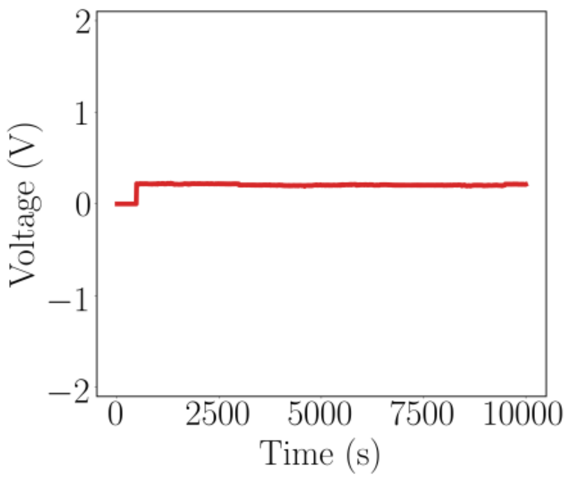

Figure 5.9: The 104 nF capacitor had a stable charge during the acquisition.

Figure (5.10) shows the sensor's voltage output under wind load without any external circuit connection to validate the values taken from the current measurement circuit.

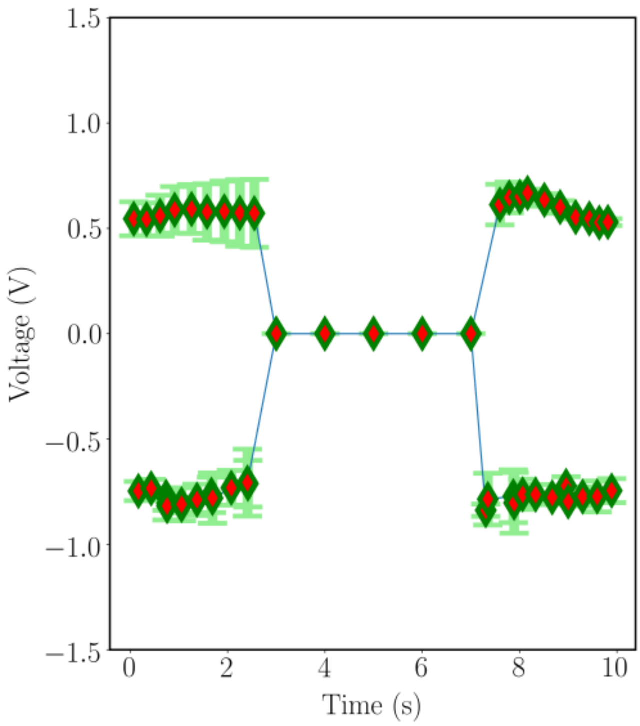

Figure 5.10: $V_{pp} = 1.74$ V was measured from the wind tests

The comparison of FEM values against values taken from the wind setup for voltage is given in Figure (5.11).

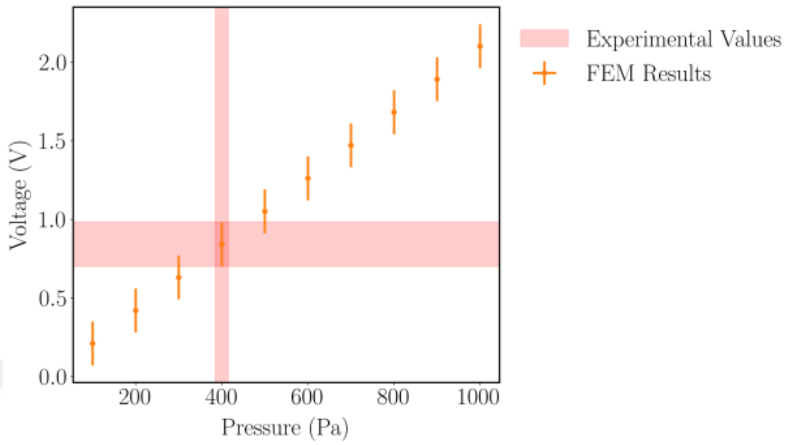

Figure 5.11: Error bars representing 10.1% error between the experimental positive maximum voltage value of 756 mV and the FEM result for pressure application 400 ± 30 Pa

The PVDF-TrFe energy harvester can run a MEMS BMP280 (Bosch) pressure sensor, widely used in structural health monitoring applications in wind turbines. The required inputs for running a BMP280 sensor are given in Table (5.1). Needing 2.7 µA current and 1.20 V voltage input, a BMP280 sensor can be run using the PVDF-TrFE energy harvester.

Table 5.1: BMP280 Properties [120].

Feature	BMP280
Footprint	2.0x2.5 mm^2
Min. V_{DDIO}	1.20 V
Current Consumption	2.7 μA
RMS Noise	1.3 Pa
Pressure Resolution	0.16 Pa
Interface	I^2 and SPI

Measurement Rate	Up to 157 Hz

Figure (5.12) reports the power and current requirements of two other commercial pressure sensors having operating voltages of 1.5 V maximum together with BMP280, showing that the PVDF-TrFe piezoelectric harvester can power these devices.

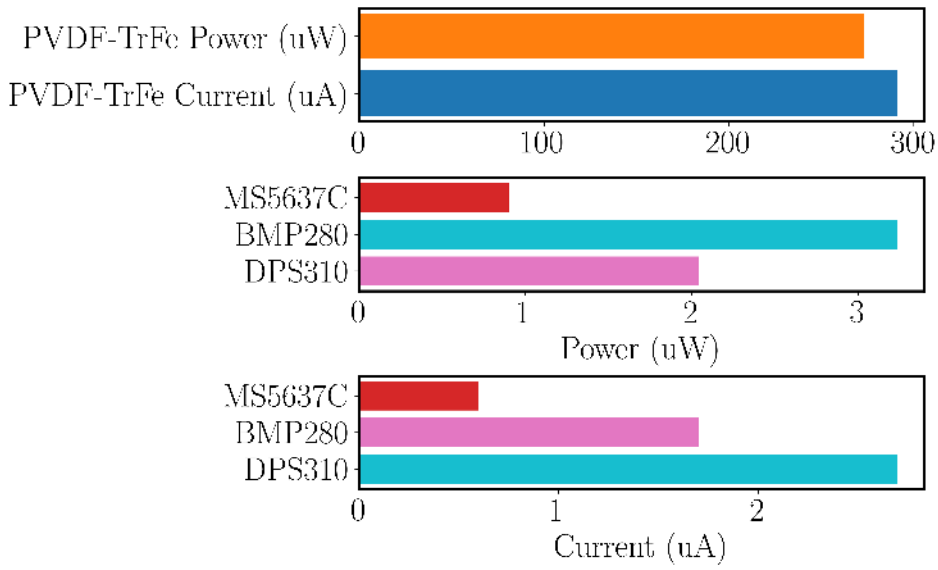

Figure 5.12: MS5637C (MEAS Switzerland), DPS310 (Infineon), and BMP280 (Bosch) are widely used commercial pressure sensors that can be powered with the harvester output [120, 121, 122].

Chapter 6

CONCLUSION

It is believed that innovations for energy harvesting would overcome problems caused by electronics' fixed-capacity power sources. This thesis presented a piezoelectric energy harvester that is adaptable and could be utilized to monitor structural components' overall health. It is feasible for autonomous sensor systems to acquire energy from the environment around them, which may subsequently be utilized to provide power.

The proposed device is meant to fulfill the prerequisites necessary for energy harvesters to function correctly. It is easy to apply using traditional methods because of its straightforward design, and it permits the creation of sensors that are relatively small in size. This study aimed to show and contrast various approaches that can be taken to analyze the suggested device. Additionally, it ascertained whether or not the proposed apparatus is a practicable alternative for energy harvesting in wind turbines. The thickness of the PVDF-TrFe material and its pyroelectric and ferroelectric properties were measured and used to characterize the material. Variations in pressure were brought about due to the dry air passage toward the fan's spinning propeller. Two proposed transducers measured as 10x10 mm^2.

Power output and mechanical reliability increase when a component can withstand high strain levels. Piezoelectric materials can sustain substantial strain, another essential feature to consider. The PVDF-TrFe energy harvester can power a MEMS BMP280 (Bosch) pressure sensor, which is a sensor that is frequently utilized in structural health monitoring applications in wind turbines. In capacitor charging experiments, the average voltage increase for a single impulse was measured to be 174 mV as the maximum. The force delivered to the piezoelectric element is directly proportional to this value.

Soft and flexible PVDF-TrFE polymer provides benefits over other ferroelectrics.

This study described the design, construction, and characterization of PEHs with PVDF-TrFE layers. The proposed PEH structures were thin films with circular plates of 1.5 mm. The neutral axis lies outside the active piezoelectric layers. The thickness of the PEH designs was 223 µm after fabrication. On an impulse load, the maximum harvested voltage was measured at 6.61 V and the current measured at 273 µA, while on a wind load, the maximum harvested voltage was measured at 937.01 mV and the current measured at 291.34 µA giving a maximum power value of 272.99 µW for the second energy harvester design.

BIBLIOGRAPHY

[1] S. Roundy and P. K. Wright, "A piezoelectric vibration based generator for wireless electronics," *Smart Mater*, vol. 13, no. 5, pp. 1131–1142, 2004.

[2] S. R. al., "Improving power output for vibration-based energy scavengers," *IEEE Pervasive Comput.*, vol. 4, no. 1, pp. 28–36, 2005.

[3] K. Chan, M. Patel, N. Barniol, S. Bhowmick, S. Cases, and A. Wong, *Three Dimensional Modeling of Piezoelectric Micromachined Transducers Built on Top of Integrated Circuits.*

[4] A. A. L. I. Alomari, *Modelling, Fabrication and Characterization for Improved Piezoelectric Energy Harvesters.* no. July, 2016.

[5] S. Roundy, P. K. Wright, and K. S. J. Pister, "Micro-electrostatic vibration-to-electricity converters," *ASME Int*, pp. 487–496, 2002.

[6] F. Yildiz, J. Zhu, R. Pecen, and L. Guo, "Energy scavenging for wireless sensor nodes with a focus on rotation to electricity conversion," 2007.

[7] S. J. Roundy, "Energy scavenging for wireless sensor nodes with a focus on rotation to electricity conversion," 2003.

[8] H. J. Jung, S. Nezami, and S. Lee, "Power supply switch circuit for intermittent energy harvesting," *Electron.*, vol. 8, p. 12, 2019.

[9] M. E. Martinez, *Polymeric Pvdf Fibers for Piezoelectric Applications in Energy Harvesting.* The University of Texas Rio Grande Valley, 2019.

[10] C. Boller, "Structural health monitoring – its association and use," in *New Trends in Structural Health Monitoring, p. 73*, 2013.

[11] J. P. Lynch and R. A. Swartz, “Wireless sensors and networks for shm,” *in Structural Health Monitoring of Civil Infrastructure Systems*, vol. 94, 2009.

[12] W. Wang, X. He, X. Wang, M. Wang, and K. Xue, “A bioinspired structure modification of piezoelectric wind energy harvester based on the prototype of leaf veins,” *Sensors Actuators, A Phys.*, vol. 279, pp. 467–473, 2018.

[13] M. E. Kiziroglou and E. M. Yeatman, *Materials and techniques for energy harvesting.* Functional Materials for Sustainable Energy Applications, Woodhead Publishing: In Woodhead Publishing Series in Energy, 2012.

[14] R. Allen and J. Kovacik, “Gas turbine cogeneration—principles and practice,” *Journal of Engineering for Gas Turbines and Power*, vol. 106, pp. 725–730, 1984.

[15] T. Zhang, “Gas turbine cogeneration—principles and practice,” *J. Phys.: Conf. Ser.*, vol. 106, no. 1449 012001, 2020.

[16] A. Santhana Krishnan, C. Suslowicz, and P. Schaumont, “Secure and stateful power transitions in embedded systems,” *Journal of Hardware and Systems Security*, vol. 4, pp. 1–14, 12 2020.

[17] S. Priya and D. J. Inman, *Energy Harvesting Technologies, SpringerLink.* link.springer.com: NY, 2009.

[18] P. A. A. Laura, J. L. Pombo, and A. Susemihl, E. A., “note on the vibration of clamped-free beam with a mass at the free end,” *J. Sound and Vib.*, vol. 37, no. 2, pp. 161–168, 1974.

[19] S. Sudevalayam and P. Kulkarni, “Energy harvesting sensor nodes: Survey and implications,” *IEEE Communications Surveys Tutorials*, vol. 13, no. 3, pp. 443–461, 2011.

[20] J. Taneja, J. Jeong, and D. Culler, "Design, modeling, and capacity planning for micro-solar power sensor networks," in *Proc. 7th International Conference on Information Processing in Sensor Networks*, 2008, pp. 407–418.

[21] A. Kansal and M. B. Srivastava, "An environmental energy harvesting framework for sensor networks," in *Proc. 2003 International Symposium on Low Power Electronics and Design.* ACM, 2003, pp. 481–486.

[22] A. Kansal, J. Hsu, S. Zahedi, and M. B. Srivastava, "Power management in energy harvesting sensor networks," *Trans. Embedded Computing Systems*, vol. 6, p. 4, 2007.

[23] J. Hsu, S. Zahedi, A. Kansal, M. Srivastava, and V. Raghunathan, "Adaptive duty cycling for energy harvesting systems," in *Proc. 2006 International Symposium on Low Power Electronics and Design.* ACM, 2006, pp. 180–185.

[24] F. Qian, M. R. Hajj, and L. Zuo, "Bio-inspired bi-stable piezoelectric harvester for broadband vibration energy harvesting," *Energy Conversion and Management*, vol. 222, no. 11317, p. 4, 2020.

[25] X. Li, K. Yu, D. Upadrashta, and Y. Yang, "Multi-branch sandwich piezoelectric energy harvester: mathematical modeling and validation," *Smart Materials and Structures*, vol. 28, no. 3, p. 035010, 2019.

[26] J. M. Ramírez, C. D. Gatti, S. P. Machado, and M. Febbo, *A piezoelectric energy harvester for rotating environment using a linked E-shape multi-beam.* Extreme Mechanics Letters, 2018.

[27] H. C. Song, C. Y. Kang, S. J. Yoon, and D. Y. Jeong, "Engineered domain configuration and piezoelectric energy harvesting in 0.7pb(mg1/3nb2/3)o3–0.3pbtio3 single crystals," *Metals Mater*, vol. 18, pp. 499–503, 2012.

[28] M. A. Karami, O. Bilgen, D. J. Inman, and M. I. Friswell, "Experimental and analytical parametric study of single-crystal unimorph beams for vibration

energy harvesting. ieee trans. ultrason," *Ferroelectr. Freq*, vol. 58, pp. 1508–1520, 2011.

[29] M. Sobocinski, M. Leinonen, J. Juuti, and H. Jantunen, "Monomorph piezoelectric wideband energy harvester integrated into ltcc," *J. Eur*, vol. 31, pp. 789–794, 2011.

[30] F. Khameneifar, S. Arzanpour, and M. A. Moallem, "Piezoelectric energy harvester for rotary motion applications: Design and experiments," *IEEE ASME Trans. Mechatron*, vol. 18, pp. 1527–1534, 2013.

[31] A. Hajati and S. G. Kim, "Ultra-wide bandwidth piezoelectric energy harvesting," *Appl. Phys. Lett*, vol. 99, p. 083105, 2011.

[32] X. Li, D. Upadrashta, K. Yu, and Y. Yang, "Sandwich piezoelectric energy harvester: Analytical modeling and experimental validation," *Energy Conversion and Management*, vol. 176, pp. 69–85, 2018.

[33] D. Upadrashta and Y. Yang, "Trident-shaped multimodal piezoelectric energy harvester," *Journal of Aerospace Engineering*, vol. 31, no. 5, p. 04018070, 2018.

[34] X. Rui, Y. Li, Y. Liu, X. Zheng, and Z. Zeng, "Experimental study and parameter optimization of a magnetic coupled piezoelectric energy harvester," *Applied Sciences*, vol. 8, no. 12, p. 2609, 2018.

[35] F. Liu, A. Phipps, S. Horowitz, K. Ngo, L. Cattafesta, T. Nishida, and J. A. M. Sheplak, "Soc," *Am.*, vol. 123, p. 1983, 2008.

[36] P. Mandurino, G. B. Bianc, and R. Garbin, "Proc," *SPEI*, vol. 4331, pp. 408–419, 2001.

[37] A. Toprak and O. Tigli, "Piezoelectric energy harvesting: State-of-the-art and challenges," *Applied Physics Reviews*, vol. 1, no. 3, p. 031104, 2014.

[38] E. Hasler, L. Stein, and G. Harbauer, "Ferroelectrics 60(1)," pp. 277–282, 1984.

[39] M. Umeda, K. Nakamura, and S. Ueha, "Jpn," *J. Appl. Phys., Part*, vol. 1, no. 35, pp. 3267–3273, 1996.

[40] N. S. Shenck and I. M. . J. A. Paradiso, pp. 30–42, 2001.

[41] P. Glynne-Jones, S. Beeby, and I. P. S. N. White, "Meas," *Technol.*, vol. 148, no. 2, pp. 68–72, 2001.

[42] E. Minazara, D. Vasic, F. Costa, and G. Poulin, "Ultrasonics 44," *e*, vol. 699, 2006.

[43] H. W. Kim, A. Batra, S. Priya, K. Uchino, D. Markley, R. E. Newnham, and H. F. Hofmann, "Jpn," *J. Appl. Phys., Part*, vol. 1, no. 43, pp. 6178–6183, 2004.

[44] T.-B. Xu, E. J. Siochi, J. H. Kang, L. Zuo, W. Zhou, X. Tang, and X. Jiang, "Smart mater," *Struct.*, vol. 22, no. 6, p. 065015, 2013.

[45] Z. Cao, J. Zhang, and H. Kuwano, "Design and characterization of miniature piezoelectric generators with low resonant frequency," *Sensors and Actuators A: Physical*, vol. 179, pp. 178–184, 2012.

[46] S. Mehraeen, S. Jagannathan, and K. A. Corzine, "Energy harvesting from vibration with alternate scavenging circuitry and tapered cantilever beam," *IEEE Transactions on Industrial Electronics*, vol. 57, no. 3, pp. 820–830, 2010.

[47] P. Becker, E. Hymon, B. Folkmer, and Y. Manoli, "High efficiency piezoelectric energy harvester with synchronized switching interface circuit, procedia engineering, volume 47," *p*, vol. 394, pp. 1877–7058, 2012. [Online]. Available: https://doi.org/10.1016/j.proeng.2012.09.166

[48] D. Guyomar and M. Lallart, “Piezoelectric conversion and energy harvesting enhancement by initial energy injection,” *Applied Physics Letters*, vol. 97, p. 014104, 2010.

[49] K. Morimoto, I. Kanno, K. Wasa, and H. Kotera, “High-efficiency piezoelectric energy harvesters of c-axis-oriented epitaxial pzt films transferred onto stainless steel cantilevers,” *Sensors and Actuators A: Physical*, vol. 163, no. 1, pp. 428–432, 2010.

[50] S. B. Horowitz, M. Sheplak, L. N. Cattafesta, and T. Nishida, “A mems acoustic energy harvester,” *Journal of Micromechanics and Microengineering*, vol. 16, no. 9, pp. S174–S181, 2006.

[51] X. Wang, J. Song, J. Liu, and Z. L. Wang, “Science 316(5821),” pp. 102–105, 2007.

[52] Y. Hu, Y. Zhang, C. Xu, L. Lin, R. L. Snyder, and Z. L. Wang, “Nano lett. 11(6),” pp. 2572–2577, 2011.

[53] Y. Hu, C. Xu, Y. Zhang, L. Lin, R. L. Snyder, and Z. L. Wang, “Adv,” *Mater.*, vol. 23, no. 35, pp. 4068–4071, 2011.

[54] L. Lin, Y. Hu, C. Xu, Y. Zhang, R. Zhang, X. Wen, and Z. L. Wang, “Nano energy 2(1),” pp. 75–81, 2013.

[55] Q. Tang, Q. He, M. Li, C. Dong, D. Xu, and X. Li, “Wireless alarm microsystem self-powered by vibration-threshold triggered energy-harvester,” *IEEE Transactions on Industrial Electronics*, pp. 1–1, 2015.

[56] S. Kihlberg, “Biodynamic response of the hand-arm system to vibration from an impact hammer and a grinder,” *Int. J. Ind. Ergonom.*, vol. 16, no. 1, pp. 1–8, July 1995.

[57] M. K. Gupta, S.-W. Kim, and B. K. Acs, "Applied materials interfaces 2016 8 (3)," pp. 1766–1773.

[58] M. Defosseux, M. Allain, P. Ivaldi, E. Defay, and S. Basrour, *Highly efficient piezoelectric micro harvester for low level of acceleration fabricated with a CMOS compatible process. 2011 16th International Solid-State Sensors.* Actuators and Microsystems Conference, 2011.

[59] M. Deterre, E. Lefeuvre, Y. Zhu, M. Woytasik, B. Boutaud, and R. D. Molin, "Micro blood pressure energy harvester for intracardiac pacemaker," *Journal of Microelectromechanical Systems*, vol. 23, no. 3, pp. 651–660, 2014.

[60] T. Galchev, E. Aktakka, and K. Najafi, "A piezoelectric parametric frequency increased generator for harvesting low-frequency vibrations. microelectromech. syst., vol. 21, no. 6, pp. 1311–1320, dec. 2012."

[61] E. S. Leland, C. T. Sherman, P. Minor, R. M. White, and P. K. Wright, *A new MEMS sensor for AC electric current*, vol. 2010, 2010.

[62] Y. Cui, Q. Zhang, M. Yao, W. Dong, and S. Gao, "Vibration piezoelectric energy harvester with multi-beam," *AIP Advances*, vol. 5, no. 4, p. 041332, 2015.

[63] G. Tang, B. Yang, C. Hou, G. Li, J. Liu, X. Chen, and C. Yang, "A piezoelectric micro generator worked at low frequency and high acceleration based on pzt and phosphor bronze bonding," *Scientific Reports*, vol. 6, p. 1, 2016.

[64] Y. Purusothaman, N. R. Alluri, A. Chandrasekhar, and S.-J. Kim, "Photoactive piezoelectric energy harvester driven by antimony sulfoiodide (sbsi): A avbvicvii class ferroelectric-semiconductor compound, nano energy," *Volume*, vol. 50, pp. 2211–2855, 2018. [Online]. Available: https://doi.org/10.1016/j.nanoen.2018.05.058

[65] D. K. Agarwal and C. H. P. Phys, "Rev," *B*, vol. 4, pp. 1893–1902, 1971.

[66] S. E. Shelton, *Piezoelectric Micromachined Ultrasound Transducers for Air-coupled Applications.* University of California Davis, 2014.

[67] J. N. Reddy, "Theory and analysis of elastic plates and shells vol. 1: Taylor and francis," vol. 2007.

[68] P. Muralt, N. Ledermann, J. Paborowski, A. Barzegar, S. Gentil, B. Belgacem, S. Petitgrand, A. Bosseboeuf, and N. Setter, "Piezoelectric micromachined ultrasonic transducers based on pzt thin films," *IEEE Trans. Ultrason., Ferroelectr., Freq*, vol. 52, pp. 2276–2288, 2005.

[69] Y. Lu, *Piezoelectric Micromachined Ultrasonic Transducers for Fingerprint Sensing.* University of California Davis, 2015.

[70] R. Naik, K. M., U. N., and Kumarchannaveeresh, "Directional optimization of mems piezoelectric hydrophone for underwater application," *Materials Today: Proceedings*, vol. 5, no. 1, pp. 823–829, 2018.

[71] S. A. Wilson, R. P. J. Jourdain, Q. Zhang, R. A. Dorey, C. R. Bowen, and M. Willander, "... persson, k. (2007)," *New materials for micro-scale sensors and actuators*, vol. 56, no. 1-6, pp. 1–129.

[72] S. A. Wilson, R. Jourdain, R. W. Whatmore, P. Morantz, J. Corbett, M. J. Hucker, and C. Warsop, "in: Proceedings of actuator 2006," in *10th International Conference on New Actuators.* Germany,th June, pp. 748–751: Bremen, 2006, pp. 14–16.

[73] R. Gaska, M. S. Shur, and A. D. Bykhovski, "Pyroelectric and piezoelectric properties of gan-based materials," *MRS Internet Journal of Nitride Semiconductor Research*, vol. 4, pp. 57–68, 1999.

[74] R. P. Strittmatter, R. A. Beach, J. Brooke, E. J. Preisler, G. S. Picus, and T. C. McGill, "Gan schottky diodes for piezoelectric strain sensing,"

Journal of Applied Physics, vol. 93, pp. 5675–5681, 2003. [Online]. Available: https://doi.org/10.1063/1.1558960

[75] M.-A. Dubois and P. Muralt, "Stress and piezoelectric properties of aluminum nitride thin films deposited onto metal electrodes by pulsed direct current reactive sputtering," *Journal of Applied Physics*, vol. 89, no. 11, pp. 6389–6395, 2001.

[76] E. Iborra, M. Clement, J. Sangrador, A. Sanz-Hervas, L. Vergara, and M. Aguilar, "Effect of particle bombardment on the orientation and the residual stress of sputtered aln films for saw devices," *IEEE Transactions on Ultrasonics, Ferroelectrics and Frequency Control*, vol. 51, no. 3, pp. 352–358, 2004.

[77] S. Trolier-Mckinstry and P. Muralt, "Thin film piezoelectrics for mems," *Journal of Electroceramics*, vol. 12, no. 1, pp. 7–17, 2004.

[78] S. C. Ko, Y. C. Kim, S. S. Lee, S. H. Choi, and S. R. Kim, "Sens," *Actuators A*, vol. 103, p. 130, 2003.

[79] P. K. Panda, "Review: environmental friendly lead-free piezoelectric materials," *Journal of Materials Science*, vol. 44, no. 19, pp. 5049–5062, 2009.

[80] T. Takenaka and H. Nagata, *J Eur Ceram Soc*, vol. 25, p. 2693, 2005.

[81] Y. M. Li, W. Chen, Q. Xu, J. Zhou, H. Sun, and M. Liao, *Ceram Int*, vol. 31, p. 139, 2005.

[82] Y. Huseyin, T. Susan, and M. Gary, *J Electro Ceram*, vol. 11, p. 217, 2003.

[83] K. Matsuo, R. J. Xie, Y. Akimune, and T. Sugiyama, *J Ceram Soc Jpn*, vol. 110, p. 491, 2002.

[84] P. D. Martin, A. Castro, P. Millan, and B. J. Enez, *J Mater Res*, vol. 13, p. 2565, 1998.

[85] P. K. Patro, A. R. Kulkarni, S. M. Gupta, and C. S. Harendranath, “In: Kharat dk (ed) national seminar on advances in electroceramics (nsae-2006), armament research development establishment, pune, india,” pp. 146–153, 2006.

[86] J. S. Harrison and Z. Ounaies, “Piezoelectric polymers encyclopedia of polymer science and technology (new york: Wiley),” pp. 474–98, 2002.

[87] T. R. Dargaville, M. C. Celina, J. M. Elliott, P. M. Chaplya, G. D. Jones, D. M. Mowery, and R. A. Assink, “Clough r l and martin j w 2005 characterization, performance and optimization of pvdf as a piezoelectric film for advanced space mirror concepts (livermore, ca: Sandia national laboratories) no,” *SAND*, vol. 20056846.

[88] K. S. Ramadan, D. Sameoto, and S. Evoy, “A review of piezoelectric polymers as functional materials for electromechanical transducers,” *Smart Materials and Structures*, vol. 23, no. 3, p. 033001, 2014.

[89] A. Safari, *Janas V F and Bandyopadhyay ADevelopment of finescale piezoelectric composites for transducers AICHE J.*, vol. 43, pp. 2849–56, 1997.

[90] F. Levassort, M. Lethiecq, and R. Desmare, “Effective electroelastic moduli of 3-3(0-3) piezocomposites ieee trans,” *Ultrason. Ferroelectr. Freq*, vol. 46, pp. 1028–34, 1999.

[91] R. Guinovart-Diaz, J. Bravo-Castillero, R. Rodriguez-Ramos, F. Sabina, and R. Martinez-Rosado, “Overall properties of piezocomposite materials 1–3 mater,” *Lett.*, vol. 48, pp. 93–8, 2001.

[92] R. Kar-Gupta and T. Venkatesh, *Electromechanical response of*, vol. 1, pp. 1093–108, 2007.

[93] R. Gerhard-Multhaupt, “Less can be more. holes in polymers lead to a new

paradigm of piezoelectric materials for electret transducers ieee trans," *Dielectrics and Electrical Insulation*, vol. 9, pp. 850–9, 2002.

[94] S. Bauer, R. Gerhard-Multhaupt, and G. M. Sessler, "Ferroelectrets: soft electroactive foams for transducers phys," *Today*, vol. 57, p. 37, 2004.

[95] P. Ueberschlag, "Pvdf piezoelectric polymer," *Sensor Review*, vol. 21, no. 2, pp. 118–126, 2001. [Online]. Available: https://doi.org/10.1108/02602280110388315

[96] B. Mohammadi, A. A. Yousefi, and S. M. Bellah, "Effect of tensile strain rate and elongation on crystalline structure and piezoelectric properties of pvdf thin films," *Polymer Testing*, vol. 26, no. 1, pp. 42–50, 2007.

[97] G. T. Davis, "in: T," in *T*, J. M. H. Wang and A. M. Glass, Eds. Blackie and Sons Ltd, Glasgow, USA(Chapter 3: Production of Ferroelectric Polymer Films. The Applications of Ferroelectric Polymers, 1988.

[98] R. G. Kepler and R. A. Anderson, "Ferroelectricity in polyvinylidene fluoride, j," *Appl. Phys.*, vol. 49, p. 1232, 1978.

[99] A. J. Lovinger, "Poly(vinylidene fluoride), in: D," in *Developments in Crystalline Polymers, Applied Science Publishers, London*, C. Bassett, Ed. Chapter 5, 1982.

[100] R. Hayakawa and Y. Wada, "Piezoelectricity and related properties of polymer films, adv," *Polym. Sci*, vol. 11, p. 1, 1973.

[101] M. G. Broadhurst, G. T. Davis, J. E. McKinney, and R. E. Collins, "Piezoelectricity and pyroelectricity in poly(vinylidene fluoride)— a model, j," *Appl. Phys.*, vol. 49, no. 10, p. 4992, 1978.

[102] C. K. Purvis and P. L. Taylor, "Piezoelectricity and pyroelectricity in poly(vinylidene fluoride): influence of the lattice structure, j," *Appl. Phys.*, vol. 54, p. 1021, 1983.

[103] A. Salimi and A. A. Yousefi, "Ftir studies of b-phase crystal formation in stretched pvdf films, polym," *Testing*, vol. 22, p. 699, 2003.

[104] M. Schwartz, "Encyclopedia of smart materials, vols. 1–2, wiley," *New York*, vol. 811, 2002.

[105] I. Katsouras, K. Asadi, M. Li *et al.*, "The negative piezoelectric effect of the ferroelectric polymer poly(vinylidene fluoride)," *Nature Mater*, vol. 15, pp. 78–84, 2016. [Online]. Available: https://doi.org/10.1038/nmat4423

[106] M. Lindner *et al.*, "Charged cellular polymers with ferroelectric behaviour. ieee trans," *Dielectr. Electr. Insul.*, vol. 11, pp. 255–263, 2004.

[107] V. S. Bystrov *et al.*, "Molecular modeling of the piezoelectric effect in the ferroelectric polymer poly(vinylidene fluoride) (pvdf)," *J. Mol. Model*, vol. 19, pp. 3591–3602, 2013.

[108] R. Machado, V. B. D. Santos, D. A. Ochoa, E. Cerdeiras, L. Mestres, and J. E. E. García, "dielectric and electromechanical properties of (bi0.5na0.5)tio3-batio3 piezoceramics at the morphotropic phase boundary region," *J. Alloys Compd*, vol. 690, pp. 568–574, 2017.

[109] J. Evans, *Piezoelectric-Based*. Self-Sustaining Artificial Cochlea, 2014.

[110] W. Tian, Z. Ling, W. Yu, and J. Shi, "A review of mems scale piezoelectric energy harvester," *Applied Sciences*, vol. 8, no. 4, p. 645, 2018.

[111] H. A. Kunkel, S. Locke, B. Pikeroen, and I. Trans, "Ultrason," *Ferroelect. Freq*, vol. 37, p. 316, 1990.

[112] T. Ueyama, S. Yamana, and N. Kaneko, "Sintering properties of batio3green sheets with high packing density," *Japanese Journal of Applied Physics*, vol. 26, 1987.

[113] X. Yan and J. Wen, "Study on factors influencing the performance of reactive powder concrete," *IOP Conference Series: Earth and Environmental Science*, vol. 2075, no. 10, pp. 1755–1315, 2020.

[114] D. Binh, V. Chebanenko, L. Duong, E. Kirillova, P. Thang, and A. Solov'ev, "Applied theory of bending vibration of the piezoelectric and piezomagnetic bimorph," *Journal of Advanced Dielectrics*, vol. 10, p. 10, 2020.

[115] K. Sappati and S. Bhadra, "Piezoelectric polymer and paper substrates: A review," *Sensors*, vol. 18, no. 11, p. 3605, 2018.

[116] Piezotech, "Piezoelectric films technical information."

[117] R. A. Surmenev, R. V. Chernozem, I. O. Pariy, and M. A. Surmeneva, "A review on piezo- and pyroelectric responses of flexible nano- and micropatterned polymer surfaces for biomedical sensing and energy harvesting applications," *Nano Energy*, vol. 79, no. 10544, pp. 2211–2855, 2021. [Online]. Available: https://doi.org/10.1016/j.nanoen.2020.105442

[118] T. Sharma, S.-S. Je, B. Gill, and J. X. J. Zhang, "Patterning piezoelectric thin film pvdf–trfe based pressure sensor for catheter application," *Sensors and Actuators A: Physical*, vol. 177, pp. 87–92, 2012.

[119] Z. Pi, J. Zhang, C. Wen, Z. Zhang, and D. Wu, "Flexible piezoelectric nanogenerator made of poly(vinylidenefluoride-co-trifluoroethylene) (pvdf-trfe) thin film," *Nano Energy*, vol. 7, pp. 33–41, 2014.

[120] Bosch, "Bmp280 – datasheet," 2021.

[121] T. E. Connectivity, "Ms5637c – low voltage barometric pressure sensor," 2017.

[122] Infineon, "Dps310 digital xensivtm barometric pressure sensor for portable devices," 2020.

Appendix A

Codes for mathematical modeling: `https://github.com/bkullukcu/energy-harvester`